# Frustrated and Allowed Structural Transitions at the Limits of the $BaAl_4$ Type: the (3+2)D Modulated Structure of $Dy(Cu_{0.18}Ga_{0.82})_{3.71}$

Hillary E. Mitchell Warden, Scott B. Lee, and Daniel C. Fredrickson*

Department of Chemistry, University of Wisconsin-Madison, 1101 University Avenue, Madison, Wisconsin, 53706, United States

**ABSTRACT:** While elemental substitution is the most common way of tuning properties in solid state compounds, this approach can break down in fantastic ways when the stability range of its structure type is exceeded. In this Article, we apply the Frustrated and Allowed Structural Transitions (FAST) principle to understand how structural complexity, in this case incommensurate modulations, can emerge at the composition limits of one common intermetallic framework, the $BaAl_4$ type. While the Dy-Ga binary intermetallic system contains no phases related to the $BaAl_4$ archetype, adding Cu to form a ternary system creates a composition region that is rich in such phases, including some whose structures remain unknown. We begin with an analysis of electronic and atomic packing issues faced by a hypothetical $BaAl_4$-type phase $DyGa_4$ and a $La_3Al_{11}$-type variant (in which a fraction of $Ga_2$ pairs are substituted by single Ga atoms). Through an inspection of its electronic density of states (DOS) distribution and DFT-Chemical Pressure (CP) scheme, we see that the stability of $BaAl_4$-type $DyGa_4$ is limited by an excess of electrons and overly large coordination environments around the Dy atoms, with the latter factor being particularly limiting. The inclusion of Cu into the system is anticipated to soothe both issues through the lowering of the valence electron count and the release of positive CPs between atoms surrounding the Dy atoms. With this picture in mind, we then move to an experimental investigation of the Dy-Cu-Ga system, elucidating the structure of $Dy(Cu_{0.18}Ga_{0.82})_{3.71(1)}$. In this compound, the $BaAl_4$ type is subject to a 2D incommensurate modulation ($\mathbf{q}_1 = 0.31\mathbf{a}^* + 0.2\mathbf{b}^*$, $\mathbf{q}_2 = 0.31\mathbf{a}^* - 0.2\mathbf{b}^*$), which can be modelled in the (3+2)D superspace group $Pmmm(a\beta0)000(a\text{-}\beta0)000$. The resulting structure solution contains blocks of the $La_3Al_{11}$ type, with the corners of these domains serving to shrink the Dy coordination environments. These results highlight how the addition of a well-chosen third element to a binary system with a missing–but plausible–compound ($BaAl_4$-type $DyGa_4$) can bring it to the cusp of stability with intriguing structural consequences.

## 1. INTRODUCTION

In solid state materials, the question of whether a compound exists under a certain set of conditions would seem to be a binary one. However, low-temperature routes such as flux synthesis[1,2] or metathesis,[3-5] as well as quenching from high pressure[6-8] are expanding the possible outcomes of solid state synthesis. Another phenomenon that blurs the answer to this question is the appearance of nanometer-scale blocks of simple phases in the structures of more complex ones. For instance, the cubic Samson phases $\beta$-$Mg_2Al_3$,[9] $Cu_4Cd_3$,[10,11] and $NaCd_2$[12,13] all have giant unit cells ($a > 25$ Å) containing more than 1100 atoms built from fragments of the Laves phase structures. The Mg-Al[14] and Na-Cd[15] systems, meanwhile, contain no such Laves phase on their own; the interfaces present in the more complex structures are necessary to stabilize their features. Inspired by these examples, in this Article we will explore the complex structural chemistry that emerges at the edge of a structure's stability range focusing on a common structure type, the $BaAl_4$ type.[16] Following the outlines of the Frustrated and Allowed Structural Transitions (FAST) principle,[17] we will see how the addition of the right element to a binary system lacking a $BaAl_4$-type compound can lead to a complex variant on this archetype involving a 2D incommensurate modulation.

We begin with a system where neither a $BaAl_4$-type compound nor any of its many variants and superstructures[18-21] are reported, the Dy-Ga binary system. In contrast, simply adding Cu to form the ternary Dy-Cu-Ga system creates a home for a composition space rich in $BaAl_4$-type motifs containing five phases in the $Dy(Cu/Ga)_{4-x}$ region.[22] $DyCu_{1.2}Ga_{2.8}$ is solved as a $BaAl_4$-type compound, while $Dy_3Cu_4Ga_7$ (= $DyCu_{1.33}Ga_{2.33}$) is said to crystallize in the $La_3Al_{11}$ type, a superstructure of the $BaAl_4$ type in which a fraction of $Al_2$ dumbbells are replaced by single atoms.[22] Two other structures in the series have only unit cells with no other structural data ($DyCuGa_3$ and $DyCu_{1.15}Ga_{2.85}$), and the last is solved in a distorted $BaAl_4$-type structure ($DyCu_{0.5}Ga_{3.5}$).[22] The incorporation of Cu into the system appears to unleash a diverse and as yet unelucidated structural chemistry based on the $BaAl_4$ type.

To understand the emergence of these compounds, we first apply the FAST Principle–the notion that structural deviations from a simple reference structure will be most facile when the electronic and atomic packing factors both benefit from it–to the unobserved binary compound, $BaAl_4$-type $DyGa_4$ and its defect structure $La_3Al_{11}$-type $Dy_3Ga_{11}$ to identify the issues that prevent their formation. The FAST analysis will highlight how electronic and atomic packing problems, well-known in the $BaAl_4$ type,[23-26] limit the stability of these structures for the Dy-Ga system: $DyGa_4$ is electron-rich relative to a pseudogap, and the Dy atoms are too small for their 16-coordinate environment in these structures. The removal of Ga atoms

on going to the $La_3Al_{11}$ type solves the electronic issue, but apparently does not contract the environments around the Dy sufficiently for the formation of a $Dy_3Ga_{11}$ compound.

We then experimentally investigate how the addition of Cu, with its smaller atomic size and lower electron count than Ga, partially resolves these issues in the Dy-Cu-Ga system through the synthesis and structure determination of the (3+2)D incommensurately modulated compound $Dy(Cu_{0.18}Ga_{0.82})_{3.71(1)}$. The 2D character of the modulation corresponds to a block-like pattern of $La_3Al_{11}$ domains that shrinks the Dy environments, with the incommensurability arising from the electron count constraints. This complex arrangement illustrates how the addition of a third element to stabilize a compound lying just outside the stability range for a structure type can yield intriguing structural phenomena, with the FAST principle serving as a guide bridging theory and experiment.

## 2. EXPERIMENTAL

**2.1 Electronic Structure Calculations.** The geometries of $DyGa_4$ ($BaAl_4$ type), $Dy_3Ga_{11}$ ($La_3Al_{11}$ type), $Dy_3Cu_2Ga_9$ ($La_3Al_{11}$ type), and $Dy_3Cu_4Ga_7$ ($La_3Al_{11}$ type) were optimized using GGA-DFT[27,28] and the Vienna *Ab initio* Simulation Package (VASP).[29-32] The optimization was performed in two steps: the relaxation of the ions in a fixed unit cell, followed by full structural relaxation. A 16×16×6 Γ-centered k-point grid was used for $DyGa_4$, while 6×2×5 Γ-centered k-point grids were used for $Dy_3Ga_{11}$, $Dy_3Cu_2Ga_9$, and $Dy_3Cu_4Ga_7$. The energy cut-off for $DyGa_4$ and $Dy_3Ga_{11}$ was 155.765 eV, while the Cu-containing phases required a higher energy cut-off of 273.246 eV. All calculations were done in high-precision mode using the projector augmented wave (PAW) potentials[33,34] provided with the package. The Dy_3 potential was used in all calculations, which folds 9 4f-electrons into the core. After optimization, single-point energy calculations were performed to obtain electronic band energies and projected density of states (DOS) distributions. DOS curves for each phase were then drawn using the program viewkel (a module of YAeHMOP).[35]

**2.2 DFT-Chemical Pressure (CP) Analysis.** The DFT-CP schemes of $YGa_4$ in the $BaAl_4$ type and $Y_3Ga_{11}$ in the $La_3Al_{11}$ type were calculated to assess the role of atomic packing in the formation of the title compound. Y was used as an f-electron free alternative to Dy with nearly the same radius ($r_Y$ = 180 pm vs. $r_{Dy}$ = 178 pm), electronegativity, and propensity to serve as a 3+ cation. The geometries were first optimized using LDA-DFT with the ABINIT software package[36-38] and Hartwigsen-Goedecker-Hutter norm-conserving pseudopotentials.[39] Then the kinetic energy and electron densities, as well as the local components of the Kohn-Sham potential needed to produce the 3D chemical pressure maps were obtained via single-point calculations performed at three volumes: equilibrium volume as well as slightly contracted and slightly expanded ones (±1.5%).

The ABINIT output was then used to calculate CP maps with *CPpackage2*,[40] using core unwarping with tricubic interpolation[41] and mapping of the nonlocal energies.[40] Space was partitioned into contact volumes between atom pairs using the Hirshfeld-inspired integration scheme.[41] The pressures within each contact volume were then averaged, projected onto spherical harmonics ($l \leq 4$), and visualized with the in-house MATLAB application Figuretool2.

The treatment of localized versus itinerant electrons on the Y atoms (for correct allocation of the Ewald and α energy terms)[40] was calibrated by calculating net atomic CPs for the compounds within Bader atomic volumes[42] at 80% and 120% of the equilibrium geometry to create internal pressure magnitudes so high that they could be considered to overwhelm the local differences in the coordination environments. For the contracted volume, the number of localized electrons on each Y atom was changed until all CPs were positive and of nearly equal magnitude (0.41 for $YGa_4$ and 0.475 for $Y_3Ga_{11}$); for the expanded cells, the number of localized electrons/Y atom was tuned until the CPs were equal and negative (0.02 for $YGa_4$ and 0.085 for $Y_3Ga_{11}$). The number of localized electrons/Y atom for the CP schemes centered at the equilibrium volume was then interpolated between these two values (0.215 for $YGa_4$ and 0.28 for $Y_3Ga_{11}$).

To account for electron transfer between Y and Ga, the Bader program[42-45] was used to calculate atomic charges on each atom for the core unwarping and contact volume construction steps of the CP analysis. The Bader charges were extracted from the LDA electronic structures, with the core electron densities being added to the valence density maps to construct the Bader volumes. Radial electron density profiles at a range of percentages of the Bader charge (0 to 75%) were then generated with the Atomic Pseudopotential Engine (APE).[46] The CP results presented in the main text are for 50% of the Bader charges, with the results of the other ionicities being presented (along with other computational details) in the Supporting Information

**2.3 Synthesis.** $Dy(Cu_{0.18}Ga_{0.82})_{3.71(1)}$ was synthesized via reaction of the component elements. Elemental Dy powder (filed from a Dy piece, HEFA Rare Earth Canada Co. Ltd., 99.9%), Cu powder (Strem 99.9%), and Ga ingots (Strem, 99.9%) were combined in a 1:1:3 Dy:Cu:Ga ratio in an Ar-filled glovebox. The metals were loaded into an uncapped alumina crucible (fashioned from an alumina tube plugged at one end with a cement base), placed in a fused silica ampoule which was then sealed under vacuum and placed in a muffle furnace. To reach a homogeneous liquid mixture, the reactants were heated to 1100 °C for 3 hours before being quickly cooled at a rate of 100 °C/hour to 500 °C, where the samples were annealed for 2 weeks. The reaction was ended by quenching the samples directly into ice water. The products were silvery ingots containing crystals suitable for analysis with X-ray diffraction.

**2.4 Powder X-ray Diffraction.** Portions of the samples were ground to a fine powder with an agate mortar and pestle and mounted on a zero-diffraction Si plate. The powders were analyzed with a Bruker D8 Advance Powder Diffractometer equipped with Cu Kα radiation (λ = 1.5418 Å) over a range of 2θ = 15 – 90° using increments of 0.02° and an exposure time of 0.9 s. Many of the diffraction peaks could be matched to a $ThMn_{12}$-type phase;[47] however, the strongest ones could not be assigned to any previously known structures. Instead, they could be indexed to a tetragonal unit cell with $a \approx$ 4.16 Å and $c \approx$ 9.82 Å.

**2.5 Elemental Analysis via Energy Dispersive X-ray Spectroscopy (EDS).** An EDS specimen was first prepared by embedding small pieces of the sample in epoxy and curing the suspension at 65 °C for 24 hours. The specimen was then polished to a flat surface using diamond lapping film at decreasing grit (9 μm to 0.5 μm) and coated with a 20 nm-thick layer of carbon to increase conductivity. The specimen was analyzed in a Hitachi S3400-N scanning electron microscope (SEM) equipped with an EDS detector (voltage = 30 keV). Back-scattered electron (BSE) images revealed two phases whose elemental compositions qualitatively match the known $ThMn_{12}$-type $DyCu_{5.60}Ga_{6.40}$ phase and the title compound $Dy(Cu_{0.18}Ga_{0.82})_{3.71(1)}$ (see the Supporting Information).

**2.6 Single Crystal X-ray Diffraction.** Well-faceted single crystals exhibiting a block habit were picked and then analyzed with an Oxford Diffraction Xcalibur E diffractometer equipped with a Mo Kα (λ = 0.71073 Å) sealed-tube X-ray source at room temperature. Run list generation and frame data processing were done in CrysalisPro.[48] The initial (3+2)D structure solution was obtained from the charge-flipping algorithm[49,50] as implemented in SUPERFLIP,[51] resulting in 8 symmetry distinct sites (2 Dy sites and 6 Cu/Ga mixed sites). Refinements were done on $F^2$ in Jana2006.[52]

Initial attempts to refine the structure yielded electron densities that were difficult to model. This issue was traced back to an overlap between the predicted positions satellites emanating from present main reflections (which show no satellites) and observed satellite surrounding absent main reflections. Therefore, for peak integration, a custom peak list was generated with the former positions removed using a MATLAB script (see the Supporting Information).

Because Cu and Ga are nearly indistinguishable with laboratory X-rays, all Cu/Ga sites in the structures were refined as mixed at a Cu:Ga ratio acquired

from EDS measurements. Given the number of occupational parameters involved in the occupational modulation waves, the restraint on the Cu:Ga ratio was most conveniently applied at the level of the atomic scattering form factors. The custom form factors were calculated by interpolating between the profiles for Cu and Ga defined in the International Tables for Crystallography Volume C[53] according to the Cu:Ga ratio. Full crystallographic information and more details regarding the filtering of the integration list and derivation of the scattering factors can be found in the Supporting Information.

## 3. RESULTS AND DISCUSSION

**3.1 Theoretical FAST analysis of the hypothetical binary compounds $DyGa_4$ and $Dy_3Ga_{11}$.** Even widely observed structure types, such as $BaAl_4$ and its derivatives, can be pushed to the limits of their stability with non-ideal elemental combinations. The $BaAl_4$ type populates many electropositive metal (A)–main group metal (E) systems. To give some examples, $BaGa_4$,[54] $SrGa_4$,[55] $EuGa_4$,[54] and $YbGa_4$[54] all crystallize in the $BaAl_4$ type, while $Sr_3In_{11}$[23] and $Sm_3Al_{11}$[56] crystallize in the related $La_3Al_{11}$ type.[57] The Dy-Ga phase diagram,[58] however, noticeably contains neither a $BaAl_4$-type compound nor any its derivatives. What about the combination of Dy and Ga metals, then, disfavors the formation of such phases, and how does moving to the Dy-Cu-Ga system enable a series of compounds with these structural motifs to emerge?

Previous research into compounds based on $BaAl_4$-type frameworks points to an ideal electron count of 14 electrons/A atom[24] and atomic size's role in the formation of defect structures.[23] With this in mind, let's begin with the theoretical investigation of these two factors in the missing compound $BaAl_4$-type $DyGa_4$. In Figure 1, we show the atomic packing and electronic issues such a hypothetical $AGa_4$ compound (A = Dy or Y as a computationally convenient f-electron free element with a comparable metallic radius: $r_Y$ = 180 pm vs. $r_{Dy}$ = 178 pm) would experience.

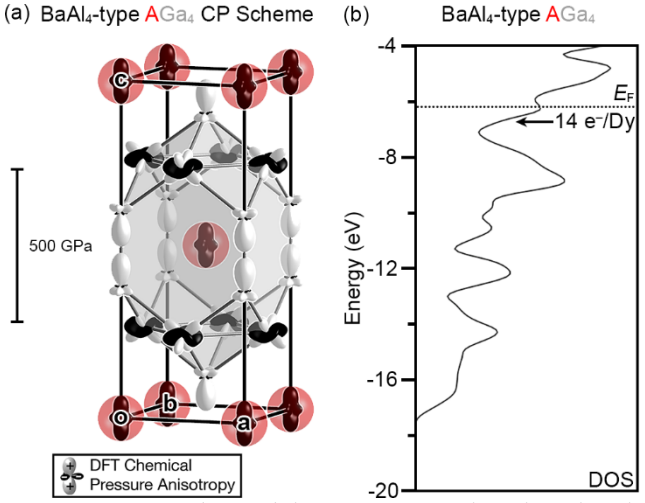


**Figure 1.** Atomic packing and electronic issues in a hypothetical $BaAl_4$-type $AGa_4$ phase. (a) The DFT-CP scheme of $AGa_4$ (with A = Y serving as an f-electron-free analogue to Dy). Here, the atomic packing tensions in the structure are viewed by resolving the macroscopic internal pressure of a structure into local two-atom pressures that call for either the expansion (positive CPs, white lobes) or contraction (negative CPs, black lobes). (b) The DOS distribution of $BaAl_4$-type $AGa_4$ (A = Dy). The Fermi energy ($E_F$) lies above a deep pseudogap. Gaussian broadening has been applied to this and the other DOS curves in this Article to emphasize their general features.

First, we examine the potential atomic packing tensions in $AGa_4$ with the DFT-Chemical Pressure (CP) analysis shown in Figure 1a. The major features of the scheme are large black ovoids indicative of overly long contacts (negative CPs) to surrounding atoms on the A atoms (shown inside red spheres). At the same time, white lobes (positive CPs) point along the Ga-Ga contacts—particularly along the Ga-Ga dumbbells—highlighting too-short distances in the Ga sublattice. This scheme reveals that the coordination environment of A (in the sense of its volume and/or coordination number) is too large; shrinking them would be favorable, if only the Ga-Ga interactions weren't already squeezed. From this picture, we can see why the $BaAl_4$ type is adopted by compounds containing A atoms with larger radii than Y or Dy, such as Ba.

The electronic density of states (DOS) distribution of $BaAl_4$-type $AGa_4$ (Figure 1b) also reveals issues with the parent structure: the Fermi energy ($E_F$) at the boundary between filled and unfilled states lands squarely on a peak of the DOS curve above the pseudogap at -9 to -7 eV (these major features are invariant whether Dy or Y is used in the calculation, as shown in the Supporting Information). The population of states above the pseudogap suggests that $DyGa_4$ has an excess of electrons. In fact, as elucidated by Zheng and Hoffmann,[24] bonding in the $BaAl_4$ type is optimized with the population of three 5 center-2 electron molecular orbitals in each of the two square nets of Ga atoms at $z$ = ¼ and ¾ (12 electrons/f.u.) and a 2 center-2 electron bond along the dumbbell contacts (2 electrons/f.u.). This amounts to 14 electrons/A atom. Indeed, the pristine $BaAl_4$ type is almost exclusively limited to compounds with 14 electrons/A atom (e.g. $BaAl_4$ and high-temperature $CaAl_4$).

How might the electronic and atomic packing problems of $AGa_4$ be addressed through modifications to the structure? One avenue is illustrated by the $La_3Al_{11}$ type: replacing ⅓ of the Ga dumbbells by a single Ga atom shrinks the A coordination environment while simultaneously lowering the electron count of the compound. The tightening of the A atom coordination here has been invoked to explain the formation of $La_3Al_{11}$-type compounds such as $Sr_3In_{11}$.[23]

We earlier illustrated how such a transition provides CP relief in the La-Al system, leading to $La_3Al_{11}$, the prototype phase for this structure type.[40] Such indeed is expected to apply for the Dy-Ga system as shown in Figure 2a with the CP scheme of the hypothetical compound $A_3Ga_{11}$ (A = Y). Many of the same features from the $AGa_4$ CP scheme can be seen: the A atoms are still largely surrounded by negative pressures and the dumbbell Ga atoms still have positive pressures directed at each other. A major difference, however, can be found in the A atoms coordinated by two single Ga atoms in place of dumbbells, which tightens two of the hexagonal faces of the A coordination polyhedron to pentagons. These A atoms experience negative CPs of lower magnitude (smaller radial distance between CP surface and atomic center), with even small positive lobes forming along the contact between the A atom and the new single Ga atoms. Another improvement is seen in the CPs around the single Ga atom; instead of large positive pressures pointing along the dumbbell contact, there are newly inserted single Ga atoms that have negative CPs pointing to their neighbors in the Ga sublattice and small positive CP features along its contacts with the A atom.

The electronics of $A_3Ga_{11}$ also show an improvement over $AGa_4$, as can be seen by comparing their DOS curves (Figures 1b and 2b).

While the overall DOS distribution is similar to the 1:4 phase, including the pseudogap near 14 electrons/A atom, the lower Ga content of $A_3Ga_{11}$ results in a lower electron count. This corresponds to a motion of the $E_F$ down the DOS distribution, leading to the $E_F$ falling right at the pseudogap. At 14 electrons/A atom, $A_3Ga_{11}$ appears to have reached a near ideal electron count.

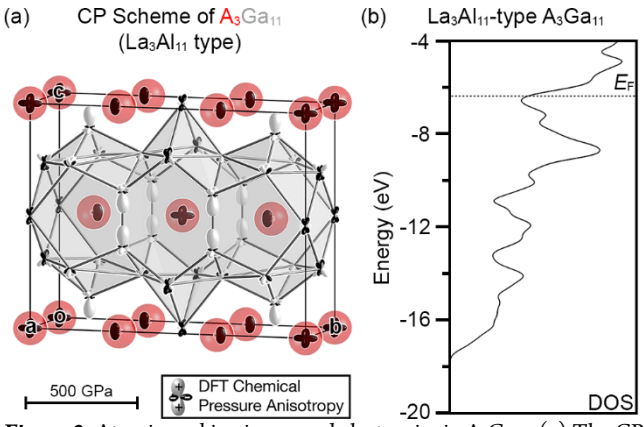


**Figure 2.** Atomic packing issues and electronics in $A_3Ga_{11}$. (a) The CP scheme of $A_3Ga_{11}$, where A = Y is used as an f-electron free proxy for Dy. (b) The DOS distribution of $A_3Ga_{11}$ (A = Dy).

Overall, then, our analysis suggests that the transformation from $AGa_4$ to $A_3Ga_{11}$ should be supported by both the electronic and atomic packing factors, making this an example of an allowed transition from the FAST perspective. This expectation is supported by total energy calculations of these phases indicating that the formation of $La_3Al_{11}$-type $Dy_3Ga_{11}$ via the reaction $3DyGa_4(s) \rightarrow Dy_3Ga_{11}(s) + Ga(s)$ is energetically favorable by -0.08 eV/atom, corresponding to -1.16 eV per dumbbell replaced (see the Supporting Information). However, the phase diagram shows no evidence of the formation of either of $DyGa_4$ or $Dy_3Ga_{11}$. Even the improvements to the atomic packing and electronics afforded by the structural transition to the $La_3Al_{11}$ type are apparently not enough to stabilize a binary Dy-Ga compound based on this framework.

**3.2 Stabilization of the $BaAl_4$-type framework by Cu incorporation.** We now turn to how Cu incorporation might bring additional stability to intermetallics based on the $BaAl_4$ type in the Dy-Ga system. First, substituting some Ga with smaller Cu atoms could enhance the size of the Dy atoms relative to their surroundings, partially offsetting their negative pressures. In addition, we saw in an earlier analysis of Cu substitution in $BaAl_4$-type $CaAl_4$ that substituting Al atoms with Cu creates opportunities for electrostatic stabilization and more intense interactions with the cations.[59] Another factor is the lower valence sp electron count of Cu than Ga (1 vs 3), which could be advantageous due to $DyGa_4$'s electron excess. In fact, moving to the composition $DyGa_{3.5}Cu_{0.5}$ would achieve the ideal electron count for a $BaAl_4$-type phase of 14 electrons/Dy atom.

One could imagine then that substantial stabilization could be brought to the Dy-Ga-based $BaAl_4$-type framework by combining such benefits of Cu substitution with those of the dumbbell/single atom substitution mechanism described in the last section. However, one should note that there are complications in having both happen at once. In particular, substituting a $Ga_2$ dumbbell by a Ga single atom and replacing Ga with Cu both serve to lower the compound's valence electron count. To explore the additivity of these effects, we show in Figure 3 electronic DOS distributions for a series of phases in which we first substitute ⅓ of the dumbbells in $DyGa_4$ with single Ga atoms, as in the $La_3Al_{11}$ type, then substitute in an increasing amount of Cu.

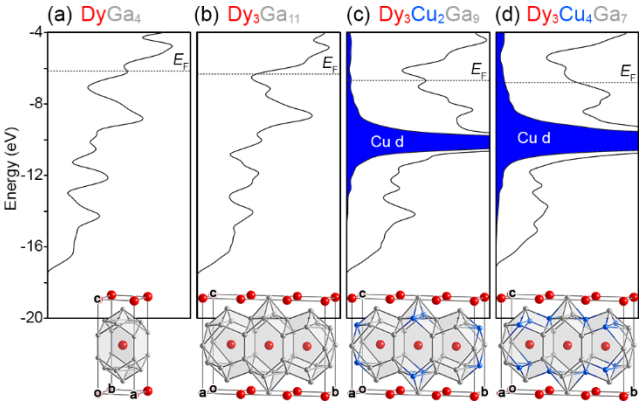


**Figure 3.** GGA-DFT DOS distributions for (a) $DyGa_4$, (b) $Dy_3Ga_{11}$, (c) $Dy_3Cu_2Ga_9$, and (d) $Dy_3Cu_4Ga_7$. In (c) and (d) the projected DOS contributions for Cu d character are shaded in blue.

We start by showing again the DOS distribution for $DyGa_4$ (15 electrons/Dy atom) in Figure 3a, with its electron-rich character shown by the $E_F$ falling on a bump above the pseudogap centered at ca. -8 eV. Transitioning to $Dy_3Ga_{11}$ (14 electrons/Dy atom), as shown in Figure 3b, lowers the $E_F$ so that it falls into the pseudogap (which is now somewhat shallower). At this point, we have reached what appears to be an electron-precise compound. However, the absence of such a phase in the Dy-Ga system suggests that removing $DyGa_4$'s electron excess by moving to $Dy_3Ga_{11}$ is not enough to form a binary compound.

Let's now introduce Cu into the $La_3Al_{11}$-type structure. First, in Figure 3c, we present the DOS curve for the hypothetical phase $Dy_3Cu_2Ga_9$. The DOS now has a large block of Cu d states at ca. -11 to -9 eV, as well as a narrower pseudogap. For our purposes, though, the most important change is that the lower electron count (12.67 electrons/Dy atom) places the $E_F$ below the pseudogap, suggesting a slight electron deficiency. Indeed, adding even more Cu, as in $Dy_3Cu_4Ga_9$ (Figure 3d), shifts the $E_F$ further below the pseudogap. Restoring the $E_F$ to its original position while maintaining this level of Cu substitution would require another source of electrons, the most obvious being the reversal of some of the dumbbell/single atoms substitutions. In this way, the goal of maintaining an electron count near 14/Dy atom will mean that the dumbbell/single atom and Ga/Cu substitution will tend to limit each other.

**3.3 Synthesis of $Dy(Cu_{0.18}Ga_{0.82})_{3.71(1)}$.** In our FAST analysis of the electronic and atomic packing issues affecting the $BaAl_4$-type framework, we saw that the Dy-Cu-Ga system sets up an intriguing conflict. Both dumbbell/single atom and Ga/Cu substitutions should soothe the challenges to the formation of a $BaAl_4$-type $DyGa_4$ phase. However, their overlapping electronic effects place constraints on the degree to which they can coexist within the same compound. To see how the structural chemistry of this system balances these effects, we now turn to an experimental foray into compounds of the form $Dy(Cu/Ga)_{4-x}$.

We began by attempting to synthesize $DyCuGa_3$, for which a unit cell ($a$ = 4.096 Å, $b$ = 4.157 Å, $c$ = 9.96 Å) but no other structural data has been reported.[22] To synthesize $DyCuGa_3$, we combined the elemental metals in a 1:1:3 Dy:Cu:Ga ratio, heated the mixed metals to

1100 °C to reach a homogeneous liquid mixture, and then annealed the sample at 500 °C for 2 weeks. These syntheses each resulted in a silvery ingot whose powder X-ray diffraction pattern contained peaks attributable to $DyCu_{5.6}Ga_{6.4}$ ($ThMn_{12}$ type); however, many of the strongest reflections matched no known intermetallic compound, or any of the relevant oxides, hydrides, or hydroxides (see the Supporting Information).

To investigate whether this unidentified phase is a member of the $Dy(Cu/Ga)_{4-x}$ series, we imaged the sample via back-scattered electron imaging (BSE) and analyzed its composition with energy-dispersive X-ray spectroscopy (EDS). The BSE images reveal two phases in the sample: a phase appearing darker gray with composition $Dy_{1.00(3)}Cu_{5.7(1)}Ga_{6.5(1)}$ matching the $ThMn_{12}$-type phase we identified in the powder X-ray diffraction data and a phase with composition $Dy_{1.00(2)}Cu_{0.70(2)}Ga_{3.19(2)}$. It seems, then, that we have successfully synthesized a compound belonging to the $Dy(Cu/Ga)_{4-x}$ family, which we will refer to as $Dy(Cu_{0.18}Ga_{0.82})_{3.71(1)}$ (from the structure refinement described below). From the EDS data, though, the Cu incorporation is less than expected from the nominal loading composition, with the excess Cu going to the formation of $DyCu_{5.6}Ga_{6.4}$.

**3.4 Diffraction Patterns of $Dy(Cu_{0.18}Ga_{0.82})_{3.71(1)}$.** Let's now turn to single crystal X-ray diffraction to uncover the structure of this new compound and how it relates to the parent $BaAl_4$ structure type. Unit cell runs of crystals picked from this sample consistently returned either a tetragonal $BaAl_4$-type cell ($a \approx 4.2$ Å, $c \approx 9.8$ Å) or an orthorhombic cell with $a \approx 5.9$ Å, $b \approx 9.8$ Å, and $c \approx 11.74$ Å that qualitatively matches the expectations for a $La_3Al_{11}$-type cell, but curiously never resulted in the orthorhombic unit cell previously reported for $DyCuGa_3$. Longer experiments to collect full hemispheres of reciprocal space invariably yielded a $BaAl_4$-type cell accounting for approximately half of the observed reflections, a sign that these crystals are consistently twinned or home to greater complexity than the simple $BaAl_4$ type.

However, the expectation of "complexity" hardly prepared us for what appears in the reconstructions of the reciprocal space layers for these crystals. The *hk*0 layer for one crystal is presented in Figure 4. Strong main reflections trace out a square grid of alternating present and absent spots consistent with the body-centered tetragonal cell of the $BaAl_4$ type (Figure 4a). However, these reflections are accompanied by many less intense peaks that appear to surround the absent main reflections in a twelve-fold ring (shown in the inset). These satellites indicate that the structure of $Dy(Cu_{0.18}Ga_{0.82})_{3.71(1)}$ is incommensurately modulated with what appears to be up to six different **q**-vectors.

The interpretation of these diffraction patterns thus appears complicated at first glance. Through much trial-and-error, though, we identified a relatively simple indexation. We begin with two **q**-vectors related by a mirror plane (Figure 4b, left): $\mathbf{q_1} \approx 0.31\mathbf{a}^* + 0.20\mathbf{b}^*$ (red arrow) and $\mathbf{q_2} \approx 0.31\mathbf{a}^* - 0.20\mathbf{b}^*$ (blue arrow), indexing the diffraction peaks as $\mathbf{G}_{hklmn} = h\mathbf{a}^* + k\mathbf{b}^* + l\mathbf{c}^* + m\mathbf{q_1} + n\mathbf{q_2}$. By adding and subtracting the **q**-vectors, we can form a pseudo-hexagonal coordinate system (yellow) with satellites falling on the points $(m, n)$ = (0,1), (1,0), (-1,1), (-1,0), (-1,-1), (0,-1), and (1,-1), going clockwise around the circle. This scheme accounts for about half of the satellite reflections. The remaining reflections can then be indexed by simply rotating the hexagonal grid 90° around **c***, corresponding to a second twin domain (Figure 4b, right). With this indexation, based on a (3+2)D incommensurately modulated structure containing two twin domains, we have now accounted for the full diffraction pattern.

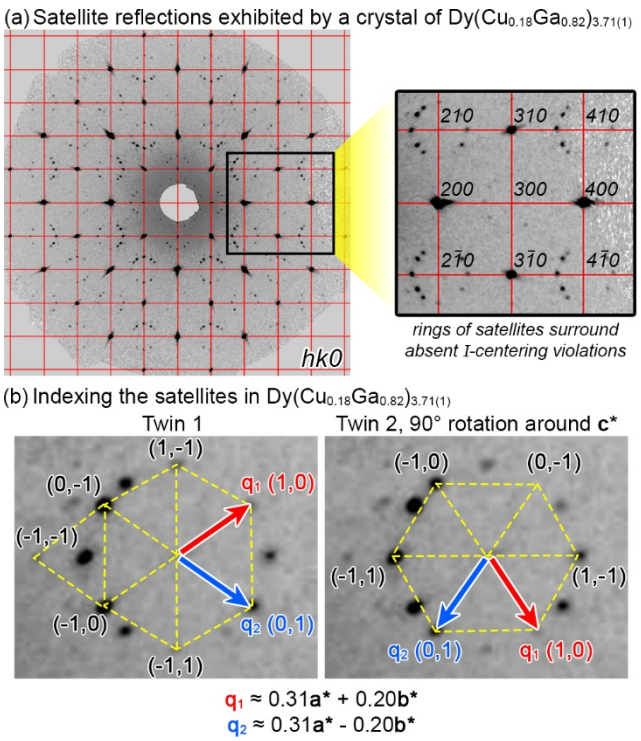


**Figure 4.** Reconstruction of the *hk*0 layer of reciprocal space in a crystal of $Dy(Cu_{0.18}Ga_{0.82})_{3.71(1)}$. (a) The *hk*0 layer of the diffraction data, with the inset highlighting the rings of satellites around absent main reflections. (b) The (3+2)D indexation of the satellites in $Dy(Cu_{0.18}Ga_{0.82})_{3.71(1)}$. All reflections are indexed as $(m, n)$ satellites originating from the absent main reflections by $m\mathbf{q_1} + n\mathbf{q_2}$, where $\mathbf{q_1} = 0.31\mathbf{a}^* + 0.20\mathbf{b}^*$ and $\mathbf{q_2} = 0.31\mathbf{a}^* - 0.20\mathbf{b}^*$ in one of two twin domains.

**3.5 $Dy(Cu_{0.18}Ga_{0.82})_{3.71(1)}$'s Average Structure.** Before we begin to incorporate the satellite reflections in our structural model, let's first consider only the main reflections. This treatment of the data will result in the average 3-dimensional structure and potentially offer us clues as to how the modulations are affecting the structure. The main reflections correspond to a body-centered tetragonal unit cell with $a \approx 4.16$ Å and $c \approx 9.82$ Å, matching a $BaAl_4$-type cell. Integration of these reflections and structural solution in the expected space group $I4/mmm$ proceeds smoothly.

The resulting structure, shown in Figure 5a, closely matches the $BaAl_4$ type with an additional atomic site at (0, 0, ½) bisecting the (Ga/Cu)-(Ga/Cu) dumbbells (refined using the custom form scattering factors described in section 2.4). The distance of the single atom and dumbbell atoms (1.18 Å) prohibits simultaneous occupation of both atomic positions, resulting in the substitution of a dumbbell of Cu/Ga atoms by a single atom, leading to a structure with dumbbells 67.6% of the time and single atoms the other 32.4%. As can be seen in Table S1 of the Supporting Information, the final refinement has acceptable R-values, e.g. $R(I>3\sigma) = 3.35$, though the GOF parameter, at 3.54, is higher than generally accepted, hinting that the model is indeed so far incomplete.

The substitution of dumbbells for single atoms recalls the superstructure of $La_3Al_{11}$, though this time the substitution does not seem

to follow a regular every-third dumbbell pattern. In fact, if we think of $BaAl_4$ and $La_3Al_{11}$ as endpoints on a spectrum of single atom substitution (from 0% to 33.3%, respectively), our average structure refinement places $Dy(Cu_{0.18}Ga_{0.82})_{3.71(1)}$ below $La_3Al_{11}$ at 32.445(8)% (Figure 5b), in line with the FAST analysis in Section 3.2. From simply considering the strongest reflections in our dataset, we already have a good idea of a source for the complexity in the (3+2)D model: the slightly lower occupation of single atoms in $Dy(Cu_{0.18}Ga_{0.82})_{3.71(1)}$ than in a periodic $La_3Al_{11}$-type structure.

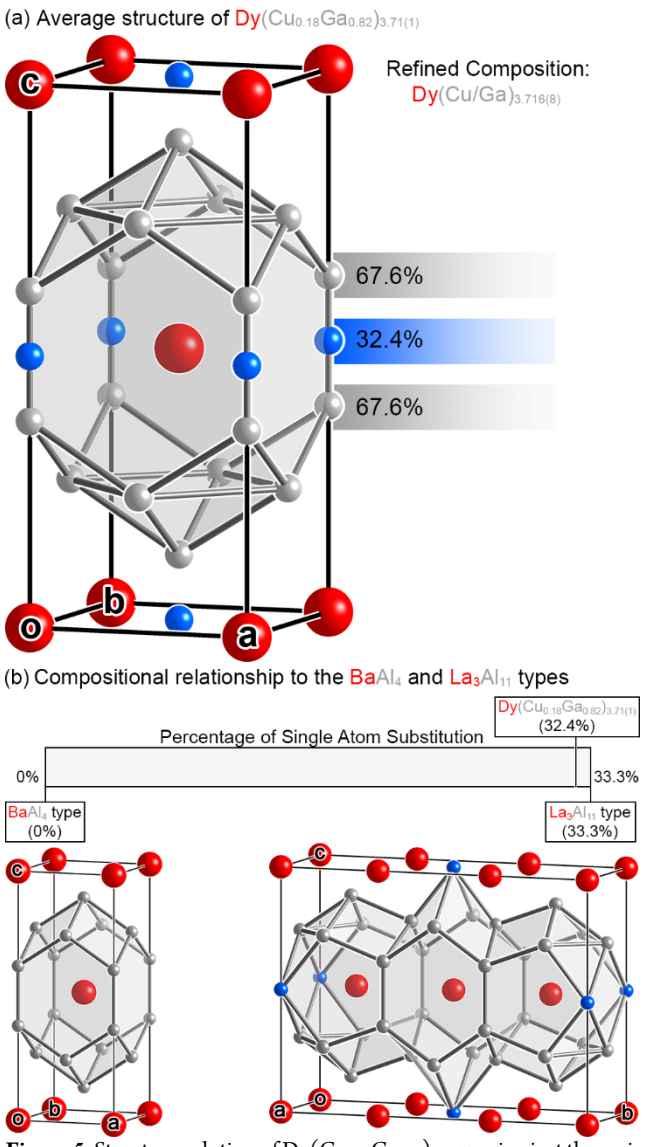


**Figure 5**. Structure solution of $Dy(Cu_{0.18}Ga_{0.82})_{3.71(1)}$ using just the main reflections. (a) $Dy(Cu_{0.18}Ga_{0.82})_{3.71(1)}$'s average structure. (b) $Dy(Cu_{0.18}Ga_{0.82})_{3.71(1)}$'s position on a spectrum from 0% dumbbell/single atom substitution ($BaAl_4$ type) to 33.3% dumbbell/single atom substitution ($La_3Al_{11}$ type).

**3.6 The (3+2)D Model of $Dy(Cu_{0.18}Ga_{0.82})_{3.71(1)}$'s Incommensurately Modulated Structure.** To uncover the details of the dumbbell/single atom substitution in $Dy(Cu_{0.18}Ga_{0.82})_{3.71(1)}$'s modulated structure, we now turn to the (3+*d*)D superspace formalism,[60,61] in which we will construct a higher-dimensional lattice using *d* additional periodic vectors to represent the phases of the modulations. In this case, this will take the form of a (3+2)D lattice where the *x*, *y*, and *z* axes of the average cell are mapped to $x_1$, $x_2$, $x_3$, and are joined by the phases of the $\mathbf{q}_1$ and $\mathbf{q}_2$ modulations, $x_4$ and $x_5$, both of which are perpendicular to physical space. Such a construction allows for a description of $Dy(Cu_{0.18}Ga_{0.82})_{3.71(1)}$'s aperiodic 3D structure in terms of a periodic (3+2)D model. To get back to a 3-dimensional picture, we then take cross-sections of superspace perpendicular to the $x_4$ and $x_5$ axes.

The first step of the structure solution is assigning the (3+2)D superspace group. We begin by considering the 3D space group of the average structure, *I*4/*mmm*, and which of its symmetry elements are compatible with the **q**-vectors. First, the 4-fold symmetry of the average tetragonal cell is broken by the off-axis **q**-vectors (see Figure 4b). This can be addressed by lowering the symmetry of the modulated structure to orthorhombic, as the **q**-vectors (as chosen) preserve the required mirror symmetry. Thus, the maximum symmetry of our modulated structure is derived from the space group *Immm*.

We must now determine whether the *I*-centering of the average structure extends in some way to the (3+2)D modulated structure. A simple extension of the body-centering, (½ ½ ½ 0 0), to the full *hklmn* set implies the condition *hklnm*: $h + k + l = 2n$, which requires that satellites surrounding absent main reflections also be absent. This is clearly violated by the distribution of satellites in the diffraction pattern. It takes closer inspection to rule out another possibility, (½ ½ ½ ½ ½), which would require the condition *hklmn*: $h + k + l + m + n = 2n$. Such a restriction would exclude cross-peaks like $(m, n) = (1,-1)$, which are distinctly present. This leaves us with *Pmmm* as the highest possible starting symmetry for the (3+2)D structure.

Moving to (3+2)D space also opens the possibility that the symmetry elements of *Pmmm* will exhibit translational components along the two newly introduced directions of periodicity, $x_4$ and/or $x_5$. For instance, the mirror plane perpendicular to **c**, which operates on a general point in 3-dimensions as $(x, y, z) \rightarrow (x, y, -z)$, could act on a point in (3+2)D space in any of four ways: $(x_1, x_2, x_3, x_4, x_5) \rightarrow (x_1, x_2, -x_3, x_4, x_5)$; $(x_1, x_2, x_3, x_4, x_5) \rightarrow (x_1, x_2, -x_3, x_4+½, x_5)$; $(x_1, x_2, x_3, x_4, x_5) \rightarrow (x_1, x_2, -x_3, x_4, x_5+½)$; or $(x_1, x_2, x_3, x_4, x_5) \rightarrow (x_1, x_2, -x_3, x_4+½, x_5+½)$. In this case, analysis of the systematic absences reveals no additional translational symmetry in the newly introduced directions. The 3D symmetry operations can thus be embedded in (3+2)D space without adding new glide components.

Combining these considerations, we can assign the maximum possible (3+2)D superspace group for $Dy(Cu_{0.18}Ga_{0.82})_{3.71(1)}$ as $Pmmm(\alpha\beta0)000(\alpha\text{-}\beta0)000$ (No. 47.2.50.68).[62-64] Here, '*Pmmm*' indicates the 3D space group from which the symmetry elements are derived, '$(\alpha\beta0)$' refers to the irrational components of $\mathbf{q}_1$, '000' means that there is no translational symmetry along $x_4$ for any of the mirror planes, and '$(\alpha\text{-}\beta0)000$' gives the corresponding information for $x_5$.

After assigning this initial superspace group, we are in principle ready to solve the structure from the integrated diffraction intensities. We then apply the charge-flipping algorithm, a method that is applicable to data of any number of dimensions, to obtain an initial structural solution. However, the electron density we obtained did not appear to be meaningful and was challenging to model. Something about our treatment of the diffraction data was evidently incorrect. Reinvestigation of the diffraction patterns uncovered a potential issue arising during integration: the $-\mathbf{q}_1+\mathbf{q}_2$ and $\mathbf{q}_1-\mathbf{q}_2$ cross-peaks stemming from the absent main reflections in the second twin

domain overlap with the predicted positions of the $\mathbf{q}_1+\mathbf{q}_2$ or $-\mathbf{q}_1-\mathbf{q}_2$ cross-peaks emanating from an observed main reflection. The integration will be unable to distinguish between these cases, effectively double counting these reflections. Using our observation that satellite reflections only surround absent main reflections, we decided to manually force the former interpretation of these reflections. We then wrote a script (provided in the Supporting Information) to remove the satellite cross-peaks originating from present main reflections (those that obey the body-centering condition *hklmn*: $h + k + l = 2n$) from the integration list generated by CrysalisPro. This removed 3228 satellites, attributing them instead to the second twin domain.

With this improved integration list, we then returned to obtaining a structure solution with the charge-flipping algorithm. The charge-flipping iterations converged on an initial (3+2)D density that matched the symmetry elements of the superspace group.

To model the electron density, we included and refined harmonic waves for the positional and ADP modulations for all atoms, as well as harmonic occupational modulations for the dumbbell/single atom sites. Although the Fourier electron density contours (see the Supporting Information), suggest that the occupational modulations might be better modeled with discontinuous functions, such as Crenel functions, only harmonic waves are offered for (3+2)D space in JANA2006. However, as has been demonstrated with the insightful analysis of $Cu_5In_3$,[65] harmonic waves can still be useful in such cases for revealing the nature of the modulation. Based on the reflections we observed in the diffraction patterns, we used the following waves in our refinement: $\mathbf{q}_1$, $\mathbf{q}_2$, $\mathbf{q}_1$-$\mathbf{q}_2$, and $\mathbf{q}_1+\mathbf{q}_2$, with no higher order harmonics.

The final refinement models the displacive modulations with four harmonic modulation waves for all eight of the atomic sites. Positional modulations of the $x_3$ coordinates of the dumbbell/single atom sites were fixed to zero to prevent correlations between the $x_3$ coordinates of the dumbbell atoms and their occupancies. For the thermal parameters, the Dy atoms were modeled with all four ADP modulation waves, while the atomic displacement parameters (ADPs) of the Cu/Ga sites except for the single atom sites were modeled with just the $\mathbf{q}_1$ and $\mathbf{q}_2$ waves.

Finally, but most importantly for the interpretation of the structure, four occupational modulation waves were applied to the dumbbell/single atom sites, restrained to be complementary such that the dumbbell/single atom occupancies on each position add up to one. An artifact of modeling the occupational waves with harmonic waves are regions where the occupancies of a dumbbell/single atom pair sum to 1 by combining numbers less than 0 and greater than 1 (see the Supporting Information). In our analysis of the structure, we will treat all occupancies for >1 or <0 as simply 1 and 0, respectively.

The final model, with the refined composition being $Dy(Cu_{0.18}Ga_{0.82})_{3.71(1)}$, has an overall $R(I>3\sigma)$ value of 3.96 (Table 1). This R-value is slightly higher than the average structure, though this is likely due to the inclusion of the many weak satellite reflections, as it is lower for the main reflections in the (3+2)D model than for the refinement of the average structure alone (3.01 vs. 3.35). In addition, we see a significant improvement in the goodness of fit, $S$(all), over the average model (1.07 vs. 3.54), and the model positions and occupations show close agreement with Fourier electron density (shown in detail in the Supporting information).

We can use cross-sections taken at different values of $x_5$ (0 and ½) to get snapshot views of how the occupations evolve over the two superspace directions. Beginning in Figure 6a, we see small Ga4 single atom occupation at $x_5 = 0$ that increases significantly as we traverse $x_5$ (Figure 6b). On the other hand, Figure 6c shows high occupancy of the Ga6 single atom site at $x_5 = 0$, which decreases along $x_5$, as shown in Figure 6d. These quick views of the occupational modulations in $Dy(Cu_{0.18}Ga_{0.82})_{3.71(1)}$ suggest that the two layers exhibit opposite behavior: when the Ga4 site is occupied, Ga6 generally isn't.

**Table 1. Crystallographic Data for $Dy(Cu_{0.18}Ga_{0.82})_{3.71(1)}$**

| | |
|---|---|
| refined composition[a] | $DyCu_{0.668}Ga_{3.046}$ $= Dy(Cu_{0.18}Ga_{0.82})_{3.71(1)}$ |
| composition from EDS | $Dy_{1.00(2)}Cu_{0.70(2)}Ga_{3.19(2)}$ |
| crystal dimensions (mm) | 0.129 × 0.052 × 0.051 |
| crystal color | silver |
| radiation source, λ (Å) | Mo K$\alpha$, 0.71073 |
| absorption correction | analytical |
| data collection temp (K) | 293 |
| (3+2)D superspace group | $Pmmm(a\beta0)000(a\text{-}\beta0)000$ |
| $a$ (Å)[b] | 4.1587(4) |
| $b$ (Å)[b] | 4.1587(4) |
| $c$ (Å) | 9.8243(13) |
| cell volume (Å$^3$) | 169.91 |
| $q_1$ | (0.31, 0.2, 0)[c] |
| $q_2$ | (0.31, -0.2, 0)[c] |
| absorption coefficient (mm$^{-1}$) | 49.396 |
| $\theta_{min}$, $\theta_{max}$ | 4.111, 28.61 |
| refinement method | $F^2$ |
| $R_{int}(I > 3\sigma$, all) | 6.47, 7.46 |
| main reflections | |
| unique reflections ($I > 3\sigma$, all) | 148, 286 |
| $R(I > 3\sigma)$, $R_w(I > 3\sigma)$ | 3.01, 8.24 |
| $R$(all), $R_w$(all) | 4.42, 8.67 |
| satellites, $(m,n)$ = (±1,0) or (0,±1) | |
| unique reflections ($I > 3\sigma$, all) | 252, 890 |
| $R(I > 3\sigma)$, $R_w(I > 3\sigma)$ | 4.78, 9.66 |
| $R$(all), $R_w$(all) | 19.68, 14.18 |
| satellites, $m = 1$, $n = 1$ | |
| unique reflections ($I > 3\sigma$, all) | 116, 503 |
| $R(I > 3\sigma)$, $R_w(I > 3\sigma)$ | 5.96, 11.83 |
| $R$(all), $R_w$(all) | 22.51, 19.97 |
| satellites, $m = 1$, $n = -1$ | |
| unique reflections ($I > 3\sigma$, all) | 132, 499 |
| $R(I > 3\sigma)$, $R_w(I > 3\sigma)$ | 6.66, 13.85 |
| $R$(all), $R_w$(all) | 26.10, 19.89 |
| overall refinement | |
| number of reflections | 25707 |
| number of parameters | 123 |
| unique reflections ($I > 3\sigma$, all) | 648, 2178 |
| $R(I > 3\sigma)$, $R_w(I > 3\sigma)$ | 3.96, 9.16 |
| $R$(all), $R_w$(all) | 12.51, 11.53 |
| $S(I > 3\sigma)$, $S$(all) | 1.67, 1.07 |
| $\Delta\rho_{max}$, $\Delta\rho_{min}$ (e$^-$/Å$^3$) | 2.80, -2.71 |

[a]The Cu:Ga ratio was calculated from the results of our EDS measurements. [b]The unit cell of the modulated structure is locked to match the *I*4/*mmm* symmetry of the average structure. [c]For the refinement, the **q**-vectors were rounded to (0.31, ±0.2, 0) to better reflect the precision with which these values are known.

When interpreting this (3+2)D model, it is helpful to focus our attention first on the dumbbell/single atom sites, as they are home to the major modulation of the full $Dy(Cu_{0.18}Ga_{0.82})_{3.71(1)}$ structure (the positional modulations of the other atoms essentially provide adaptation to whether a dumbbell or single atom occupies these sites). In moving to the (3+2)D structure from the average structure, the lower symmetry and loss of the centering vectors have a significant consequence: the dumbbell/single atom pairs centered at ($x_1$, $x_2$, $x_3$) = (½, ½, 0) (Ga3/Ga4) and ($x_1$, $x_2$, $x_3$) = (0, 0, ½) (Ga5/Ga6) become distinct crystallographic sites. We present the modeled occupational modulations of these sites in (3+2)D superspace in Figure 6, shown as cross-sections of constant $x_5$ with $x_3$ plotted against $x_4$ (with $x_3$ being vertical to match the orientation of the dumbbells in the other figures). The modeled atomic positions are shown as strings that are parallel to $x_4$, with the alternation between majority dumbbells (gray) and majority single atoms (blue) along $x_4$ corresponding to the modulated occupancies of these sites.

We can use cross-sections taken at different values of $x_5$ (0 and ½) to get snapshot views of how the occupations evolve over the two superspace directions. Beginning in Figure 6a, we see small Ga4 single atom occupation at $x_5$ = 0 that increases significantly as we traverse $x_5$ (Figure 6b). On the other hand, Figure 6c shows high occupancy of the Ga6 single atom site at $x_5$ = 0, which decreases along $x_5$, as shown in Figure 6d. These quick views of the occupational modulations in $Dy(Cu_{0.18}Ga_{0.82})_{3.71(1)}$ suggest that the two layers exhibit opposite behavior: when the Ga4 site is occupied, Ga6 generally isn't.

To look at the behavior of the single atom occupation in more detail, we show a plot of $x_4$ vs. $x_5$ centered at the Ga4 and Ga6 positions (Figures 6e and 6f, respectively). The plot shows contour maps of the single atom occupation, where blue areas have high occupation of these sites and white corresponds to low or no occupation of the sites. When we compare the Ga4 and Ga6 sites, the oppositely coordinated behavior becomes very clear, as does the mirror symmetry relating $x_4$ and $x_5$ (and the $\mathbf{q}_1$ and $\mathbf{q}_2$ vectors). In areas where one site is likely to be a single atom, the other is not. This matches our expectation from the individual plots shown in Figures 6a-d, but one other interesting feature becomes clear in these plots: the shape of the occupation is significantly different in the two layers, with the Ga4 site forming diamond shapes and the Ga6 site forming concave ovals. In the next section, we will see how these differences manifest in the structure in physical space.

**3.7 The Dumbbell/Single Atom Occupational Modulations in Physical Space.** To see how the occupational modulation functions of Figures 6e-f translate to the structure in 3D, let's map them to 2D slices of the physical structure centered at $z$ = 0 and $z$ = ½, i.e. the layers containing the single atoms and dumbbell centers. For the fractional coordinates within the layer ($x$, $y$), the phases of the modulation are given by

$$x_4(x,y) = q_{1,x}\cdot x + q_{1,y}\cdot y + t_{0,x_4} \qquad (1)$$

$$x_5(x,y) = q_{2,x}\cdot x + q_{2,y}\cdot y + t_{0,x_5} \qquad (2)$$

where $x_4$ and $x_5$ are the phases of the modulation; $q_{1,x}$, $q_{1,y}$ etc. give components of the $\mathbf{q}$-vectors, $\mathbf{q}_1$ and $\mathbf{q}_2$; and $t_{0,x4}$ and $t_{0,x5}$ are the points of intersection of physical space with the $x_4$ and $x_5$ axes, respectively. For simplicity, we can choose these intercepts to be 0 for both $x_4$ and $x_5$.

These equations result in $x_4$ and $x_5$ values that we can then use to calculate the probability of a Ga4 or Ga6 site being occupied at a point in the physical $ab$-plane at $z$ = 0 or $z$ = ½, respectively. For a miscellaneous site $j$ these take the form:

$$P_j(x_4,x_5) = \overline{occ}_j \cdot [1 + P_{1,j}\sin(2\pi x_4) + P_{2,j}\sin(2\pi x_5) + P_{3,j}\sin\big(2\pi(x_4 - x_5)\big) + P_{4,j}\sin\big(2\pi(x_4 + x_5)\big)] \qquad (3)$$

where $\overline{occ}_j$ is the average occupation of the site, and $P_{1,j}$, $P_{2,j}$, $P_{3,j}$, and $P_{4,j}$ are the modulation parameters for site $j$, tables of which can be found in the Supporting Information. By substituting equations 1 and 2 for $x_4$ and $x_5$ in equation 3, functions of the form $P_j(x, y)$ are obtained that can be visualized in the context of the 3D structure.

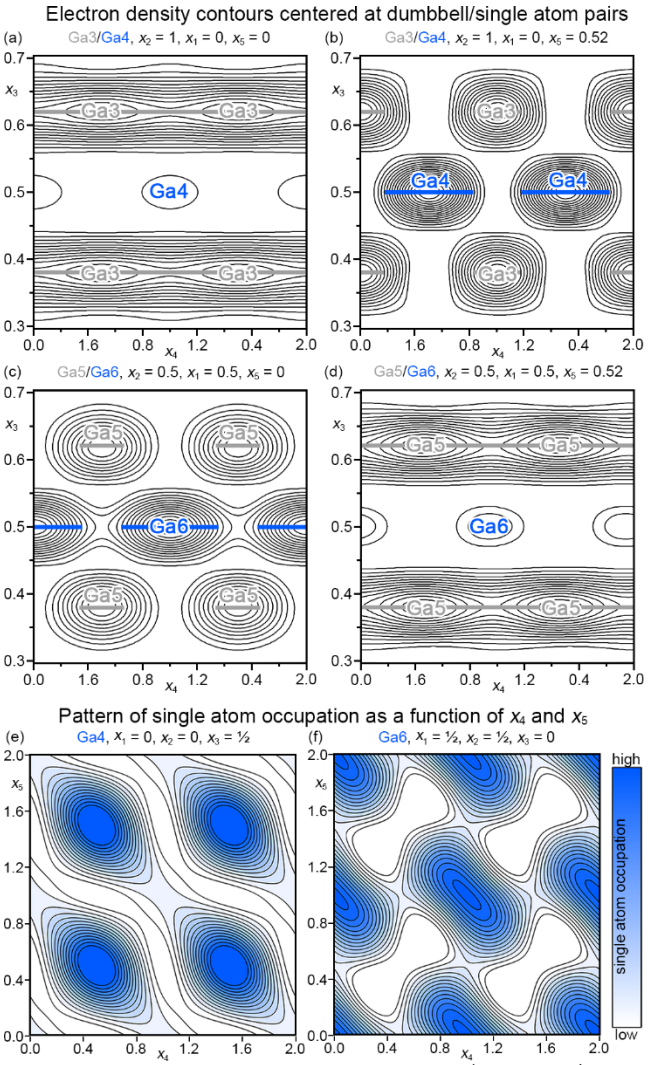


**Figure 6.** The occupational modulations of $Dy(Cu_{0.18}Ga_{0.82})_{3.71(1)}$'s dumbbell/single atom sites in (3+2)D superspace. (a) The electron density contours for the Ga3/Ga4 site pair as functions of $x_3$ and $x_4$ at $x_5$ = 0. Analogous plots are given for the (b) Ga5/Ga6 site pair at $x_5$ = 0, (c) the Ga3/Ga4 atom pair at $x_5$ = ½, and the (d) Ga5/Ga6 pair at $x_5$ = ½. In each plot, the electron density is summed over a 1 Å thick width along $x_1$ and $x_2$. Occupancy cut-off: curves are drawn for the member of the atom pair with the higher occupancy. Electron density contours: 3 electrons/Å$^3$. The patterns of single atom occupation for (e) Ga4 and (f) Ga6 as a function of the phases of the two modulations, $x_4$ and $x_5$.

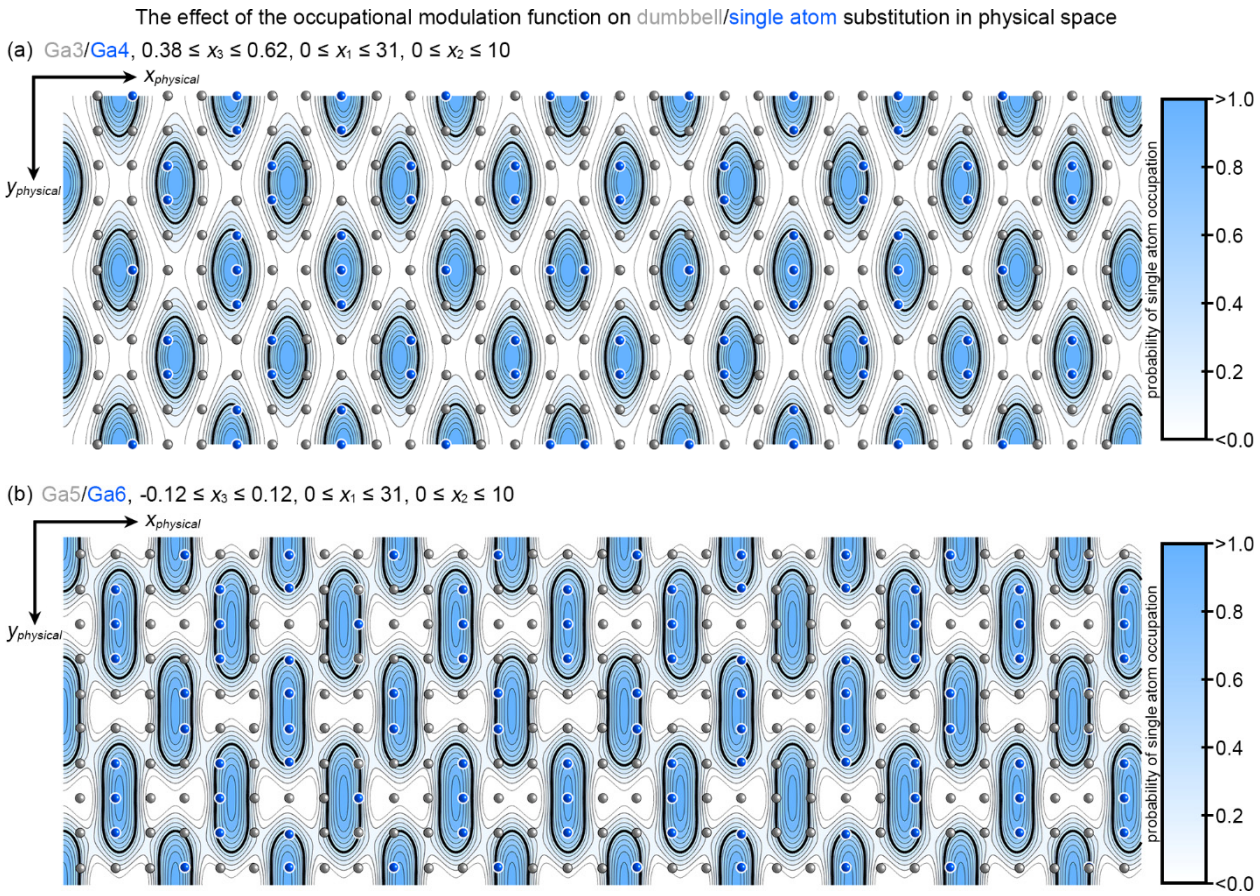


**Figure 7.** The occupational modulations of the (a) Ga3/Ga4 and (b) Ga5/Ga6 dumbbell/single atom positions viewed in physical space. Contours shown for probabilities in steps of 0.1. The thick black line is shown at probability = 0.5, the cut-off separating regions with majority dumbbell (gray spheres) occupation and those of majority single atom (blue spheres) occupation. The ranges of the gradient are set to 0 and 1, though the limits of the occupations go slightly beyond a range of 0-1 (an artifact of the harmonic model).

In Figure 7a we begin by overlaying the Ga4 occupational modulation on a layer of the structure containing the Ga4 sites in physical space. The probability of Ga4 occupation is indicated by color, with blue representing sites most likely to have a Ga4 single atom present and white indicating those sites with a low chance of Ga4 occupation (instead, a Ga3 dumbbell is expected at these sites). A thick black contour representing 50% Ga4 occupancy is also provided to mark the boundary between regions with majority Ga4 single atoms and those with majority Ga3 dumbbells. Here, the blue majority Ga4 areas are shaped like rounded diamonds and arranged in a checkerboard pattern across the plane.

Of course, while we have drawn this function as continuous, it actually only applies to the distinct positions of the Ga4/Ga3 sites, arranged in a square net in the layer. By comparing the placement of these sites relative to the modulation, the incommensurate nature of the structure becomes evident. Along *y*, five steps along the square net are required to land on an equivalent point on the modulation function, in line with $|q_{1,y}| = |q_{2,y}| = 0.2$. For the *x*-direction, three steps along the square net falls just short of a repeat vector of the modulation, corresponding to $|q_{1,x}| = |q_{2,x}| = 0.31$.

Indeed, the result of this mismatched periodicity is a real space structure that resembles a $BaAl_4$-type matrix with small islands of single atoms embedded into it. The near tripling of *a* creates a frequent motif of a single atom followed by two dumbbells along *x*, a pattern reminiscent of the $La_3Al_{11}$ type. The repeat period of the modulation wave along *x* in $Dy(Cu_{0.18}Ga_{0.82})_{3.71(1)}$ (reflecting $q_x = q_{x,1} = q_{x,2}$ being 0.31 rather the 1/3 that would apply for the $La_3Al_{11}$-type) seems closely connected to the stoichiometry of the phase. In fact, the formula obtained from the refinement, $Dy(Cu/Ga)_{3.71(1)}$, is within experimental error of $Dy(Cu/Ga)_{4-q_x}$. The *y*-component of the modulation, then, appears not to change the coverage of single atoms along the physical *y* axis (at least on the average between the Ga4 and Ga6 layers), but to break the series of lines of single atoms seen in $La_3Al_{11}$ type into a block-pattern of shorter segments.

Figure 7b shows the analogous contour for the Ga6 single atom site. Familiarly, we see a pattern that is approximately opposite to that of the Ga4 occupations, i.e. the blue areas in this layer align with the white areas in the layer above it. We also see in the physical space projection that the blue areas are differently shaped (as we saw in the electron density contours of Figure 6), forming elongated ovals arranged in a checkerboard pattern. In this case, the islands of single atom occupation are more stretched along *y*, creating an even stronger impression of $La_3Al_{11}$-type motifs and higher single atom occupancy overall. In fact, this observation matches the trends in the average probability of the single atom sites for the two layers (34.23% for Ga6 vs. 27.23% for Ga4).

This 3-dimensional view of the occupational modulations shows an interesting arrangement of familiar structural motifs. Within both

layers, there are fragments of the ordered $La_3Al_{11}$ type (a ...dumbbell-dumbbell-single atom... sequence along $x$), with the occassional variations in the number of dumbbells between single atoms. In each case, though, the $La_3Al_{11}$-type fragments are arranged in small domains that create a patchwork pattern instead of the strips of single atoms we would find in the $La_3Al_{11}$ type itself. In the next section, we'll consider how this arrangement of dumbbells and single atoms addresses the atomic packing issues we identified in the parent structure.

**3.8 Tighter Dy Coordination Environments in Modulated $Dy(Cu_{0.18}Ga_{0.82})_{3.71(1)}$.** As was anticipated in the theoretical analysis of Section 3.2, the modulation in $Dy(Cu_{0.18}Ga_{0.82})_{3.71(1)}$ appears to reduce the frequency of dumbbell/single atom substitutions relative to the $La_3Al_{11}$ type. This effect would be expected as a response to Cu's lower valence electron count as it is incorporated into the structure. However, this electronic effect alone does not explain the block-like arrangement of single atom domains in the modulated $Dy(Cu_{0.18}Ga_{0.82})_{3.71(1)}$ structure, as opposed to the strips in the $La_3Al_{11}$ type. Clues to the origins of this block morphology can be seen in the major tensions we identified in the CP schemes of $DyGa_4$ and $Dy_3Ga_{11}$ (section 3.1 and 3.2): positive pressures in the Ga sublattice (especially along the dumbbell contacts) countered by negative CPs on the Dy atoms. Combining these schemes with the observation that neither of these compounds arise in the Dy-Ga system, it seems the Dy atoms are too small for their coordination environments, even in $Dy_3Ga_{11}$, and the inclusion of the smaller atom Cu helps to tighten the Dy coordination.

It is then interesting to explore how the Dy coordination environments in $Dy(Cu_{0.18}Ga_{0.82})_{3.71(1)}$ compare to those that we would find in simpler $BaAl_4$- and $La_3Al_{11}$-type structures. Throughout this series, there are three basic coordination environments (Figure 8a), surrounding the central Dy atom with as few as 14 Ga neighbors to as many as 16. From the CP schemes of $DyGa_4$ and $Dy_3Ga_{11}$, it seems that the Dy atoms of the structures would prefer a coordination number (CN) = 14 and would like to minimize how often they are encased within 16 Ga/Cu atoms.

Let's investigate how often the different basic coordination environments occur in each of the different structures. We'll do this by plotting histograms of the number of Dy atoms with different CNs by Ga (counting atoms within a radius of 3.65 Å). Consider first a hypothetical $BaAl_4$-type $DyGa_4$ structure (Figure 8b). Here, because there is no dumbbell/single atom substitution, every Dy atom is inside a 16-coordinate polyhedra; this histogram contains a single bin centered at CN = 16. In moving to the $La_3Al_{11}$ type, the single atom substitution for every 3rd dumbbell results in two bins (Figure 8c): CN = 14 for ⅔ of the Dy atoms in the structure with the remaining ⅓ still having CN = 16. It appears, then, that even when most of the CN = 14, there is still a relatively frequent occurrence of 16-coordinate Dy atoms. Given the CP issues faced by the Dy atoms, this would certainly be destabilizing.

Making the same histogram for the modulated $Dy(Cu_{0.18}Ga_{0.82})_{3.71(1)}$ structure (using the modulated occupancies of the dumbbell/single atom sites to weight each neighbor to the Dy atoms) reveals a remarkable change (Figure 8d).[66] Rather than CNs of either 14 or 16, we now see a range that stretches between these extremes. The distribution is also significantly different from either of the parent structures, with the bin centered at CN = 16 polyhedra accounting for only 3.59% of the Dy atoms vs. 100% in the $BaAl_4$-type and 33.3% in the $La_3Al_{11}$ type. As in the $La_3Al_{11}$ type, the majority of the Dy atoms are surrounded by fewer than 15 Ga/Cu atoms, 64.94%. Now, though, a significant percentage (31.47%) have coordination numbers between 15 and 16.

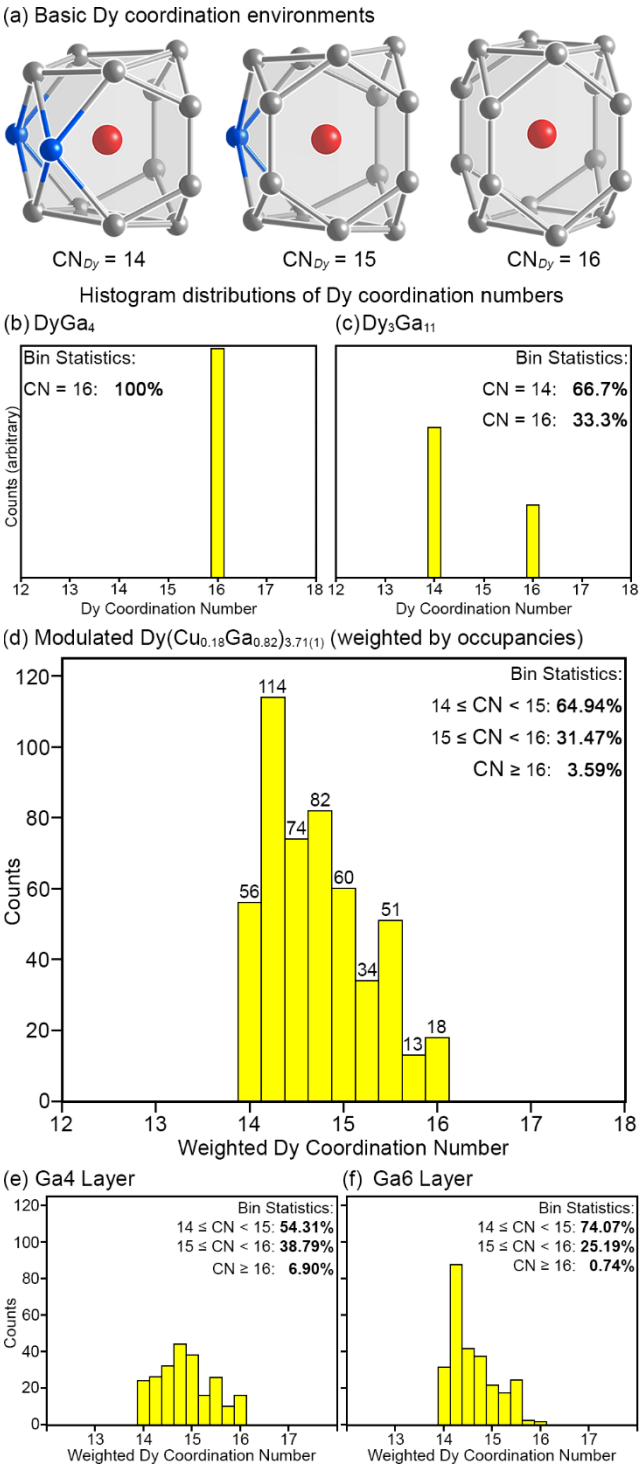


**Figure 8.** Tightening of the Dy coordination environments in the modulated $Dy(Cu_{0.18}Ga_{0.82})_{3.71(1)}$ structure. (a) The basic Dy coordination environments available to the Dy atoms. (b) Histogram distributions of Dy coordination numbers (CN) in $DyGa_4$, (c) $Dy_3Ga_{11}$, and (d) a sample of 31×10×1 basic cells of the modulated $Dy(Cu_{0.18}Ga_{0.82})_{3.71(1)}$ structure, further broken down into distributions of the two symmetry-dis-

tinct layers containing (e) Ga4 and (f) Ga6. The non-integer coordination numbers emerge for the modulated structure due to the fractional occupancies of the dumbbell/single atom sites.

Histograms such as these can also be used to inspect the symmetry-inequivalence of the layers containing the Ga4 and Ga6 single atom sites in $Dy(Cu_{0.18}Ga_{0.82})_{3.71(1)}$, the primary source for the loss of the *I*-centering in the original $BaAl_4$ type. Figures 8e and 8f present histograms for the coordination numbers of the Dy atoms located just within the Ga4 and Ga6 layers, respectively. In comparing these layers, several points of contrast become clear: there are significantly fewer Dy atoms in the CN=16 bin for the Ga6 layer (<1 % vs ~7%). At the same time, the Ga6 layer shows a large peak in the 14 to 15 range, and has an overall higher percentage within the bins centered in the range $14 \le CN < 15$ than the Ga4 layer (74.07% vs. 54.31%).

While the layers are different, they share the common feature that the number of CN = 16 Dy atoms is substantially reduced relative to either the $BaAl_4$ or $La_3Al_{11}$ types. It appears, then, that the significant tension of the parent structures–overly-large Dy coordination environments–has been alleviated in this incommensurate arrangement. How is this accomplished? To answer this question, in Figure 9, we present a projection of the $Dy_3Ga_{11}$ structure to show how the CN = 14 and CN = 16 Dy-centered polyhedra are distributed, then compare it to how the different Dy CNs are distributed in similar projections of the Ga4- and Ga6-containing layers. Here, the Dy-centered polyhedra are color-coded based on the bins whose centers lie in the ranges $14 \le CN < 15$, $15 \le CN < 16$, and $16 \le CN$, where dark gray indicates no improvement and light gray indicates significant shrinking relative to the $BaAl_4$ type.

In the $La_3Al_{11}$ structure (Figure 9a), there is a periodic arrangement of the dumbbell/single atom substitutions: along *b*, every third dumbbell becomes a single atom, forming two strips of 14-coordinate Dy atoms followed by a strip of 16-coordinate Dy atoms. In the modulated layers, remnants of strip-like domains remain, but block-like arrangements of 14- and 15-coordinate Dy atoms become prevalent. The Ga4 layer (Figure 9b) is dominated by blocks of medium gray polyhedra (CN = 15); the Ga6 layer (Figure 9c) drawn in this way reveals clusters of CN = 14, with relatively few dark gray polyhedra. The differences between layers suggests there are advantages to making an alternation of layers with higher (Ga6) and lower (Ga4) levels of dumbbell/single atom substitution.

These projections also show the primary difference in the layers of the modulated structure compared to the periodic parent structure. Instead of strips of dumbbell/single atom substitutions, the modulated structure forms a patchwork pattern of the $La_3Al_{11}$ type. These block-like arrangements are responsible for the tightened Dy coordinates in the modulated $Dy(Cu_{0.18}Ga_{0.82})_{3.71(1)}$ structure (Figure 9e): the boundaries of the $La_3Al_{11}$-type blocks provide the opportunity for CN = 15 Dy atoms, not possible in the parent structure alone.

**3.9 $Dy(Cu_{0.18}Ga_{0.82})_{3.71(1)}$'s Modulated Structure Viewed Through the FAST Principle.** As we've seen above, the tightly coupled effects of the electronic and atomic packing factors result in the modulated structure of $Dy(Cu_{0.18}Ga_{0.82})_{3.71(1)}$. We can summarize these effects schematically using an abstract potential energy surface (Scheme 1), focusing on the problems and solutions afforded by different structural variations away from a hypothetical $BaAl_4$-type $DyGa_4$ parent structure through changes in the Cu/Ga ratios and the frequency of single atom/dumbbell substitution, as represented by the *x*-component of the **q**-vectors, $q_x$.

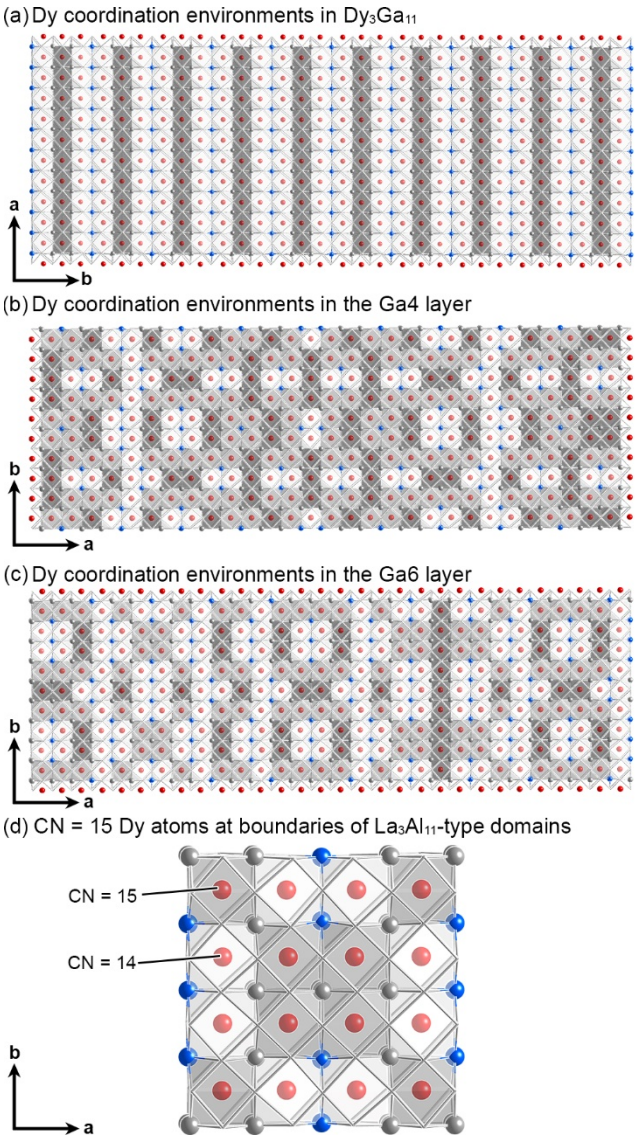


**Figure 9.** The physical space distribution of Dy CNs. (a) The distribution of Dy CNs within a layer of the $La_3Al_{11}$ type, with the tightening of the CNs compared to $DyGa_4$ indicated by the gray hues of the coordination polyhedra: light gray polyhedra, medium gray polyhedra, and dark gray polyhedra correspond Dy sites from bins with centers in the ranges $14 \le CN < 15$, $15 \le CN < 16$, and $16 \le CN$, respectively (see Figure 8). (b) The corresponding plot for the Ga4 layer of the modulated $Dy(Cu_{0.18}Ga_{0.82})_{3.71(1)}$ structure. (c) Analogous plot for the Ga6 layer. (d) Illustrating how breaks in the strings of single atoms along *y* in the $La_3Al_{11}$ type can result in CN = 15 Dy atoms.

First, we present the qualitative potential energy surface for the electronic component. Beginning in the top left corner, $BaAl_4$-type $DyGa_4$ is represented by a high-energy peak (red) reflecting its being 1 electron/Dy atom in excess of the 14-electron ideal. The transition to $La_3Al_{11}$-type $Dy_3Ga_{11}$ (low energy, blue peak) should solve the electronic issues of the $BaAl_4$ type, as the replacement of every third $Ga_2$ dumbbell by a single Ga atom lowers the electron count to this ideal value. However, the possibility of lowering the electron count via the Ga/Cu ratio stretches the minimum into a canyon that runs

diagonally from $Dy_3Ga_{11}$ (Cu/Ga ratio = 0, $q_x$ = ⅓) to $Dy(Cu_{1/8}Ga_{7/8})_4$ in the $BaAl_4$ type (Cu/Ga ratio = 1/7, $q_x$ = 0). Where does the the modulated $Dy(Cu_{0.18}Ga_{0.82})_{3.71(1)}$ phase lie on this map? Curiously, with its Cu/Ga ratio of the modulated $Dy(Cu_{0.18}Ga_{0.82})_{3.71(1)}$ phase lies on the opposite side of the canyon from the parent $DyGa_4$ phase, as its Cu/Ga ratio of 0.22 is too high for its $q_x$ value of 0.31, making the electron count lower than the 14 electrons/Dy atom target.

**Scheme 1. Qualitative Interpretation of Modulated $Dy(Cu_{0.18}Ga_{0.82})_{3.71(1)}$ in Terms of the FAST Principle**

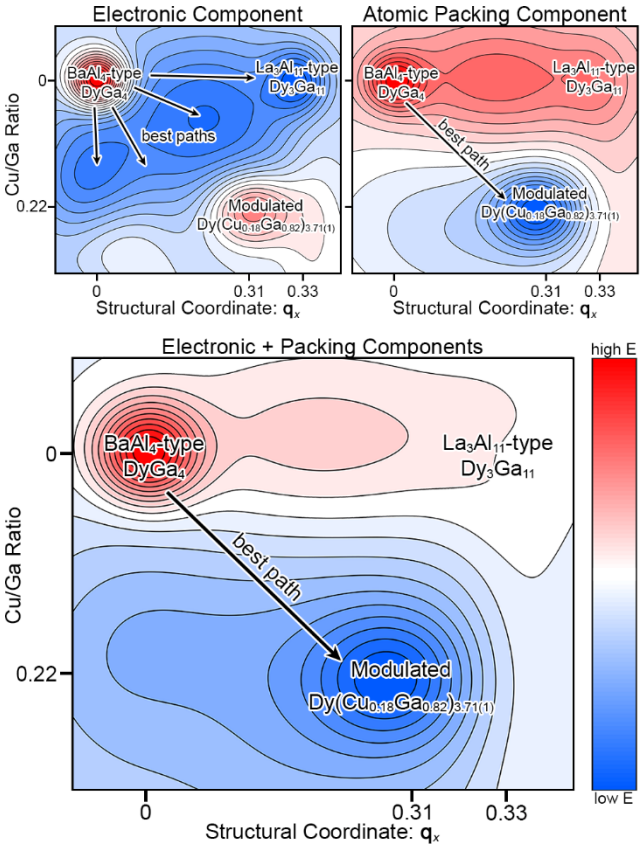


The corresponding scheme for the atomic packing component tells quite a different story. Again, the $BaAl_4$ type near the top left corner is shown as a high energy peak, reflecting the too-large coordination environments of the Dy atoms in this structure. And while the $La_3Al_{11}$ type goes some way towards solving these issues by its every-third substitution of $Ga_2$ dumbbells for single Ga atoms, the residual negative pressures on the Dy are sufficient to prevent this phase from being experimentally observed. We have thus represented it with a lighter pink indicating some improvement over the $BaAl_4$-type. Moving straight down the plot from $DyGa_4$ to Cu-substituted version of the same type also leads to some stablizing contraction around the Dy. However, the true low-energy structure comes from moving diagonally down the plot, as this combines the dumbbell/single atom and Ga/Cu substitution mechanisms. This aligns with the transition to the modulated structure of $Dy(Cu_{0.18}Ga_{0.82})_{3.71(1)}$.

By taking the sum of the qualitative energy contours for both factors, we can get an overview of how the electronic and packing components are working within this system. Overall, $BaAl_4$-type $DyGa_4$ is a high energy structure from the point of view of both factors. The transition to $La_3Al_{11}$-type $Dy_3Ga_{11}$ offers relief on both maps, but does not sufficiently resolve the atomic packing issues to result in a low-energy feature in the summed scheme. When Cu is incorporated, further relief for the packing factor becomes possible, but the electronic factor then requires the reversal of some $Ga_2$/Ga substitutions relative to the $La_3Al_{11}$ type (lower $q_x$). Overall, our experimental results suggest that the best path for relieving destabilizing $DyGa_4$ appears to be the structural transition to the observed modulated structure of $Dy(Cu_{0.18}Ga_{0.82})_{3.71(1)}$. This hints that here the atomic packing factor has a somewhat stronger weight.

## 4. CONCLUSIONS

In this Article, we have presented the synthesis and complex crystal structure of $Dy(Cu_{0.18}Ga_{0.82})_{3.71(1)}$, and explained its (3+2)D incommensurately modulated arrangement in terms of electronic and atomic packing issues preventing the formation of its simple parent structure, a $BaAl_4$-type $DyGa_4$ phase. We began with the theoretical analysis of $DyGa_4$ which reveals an excess of electrons relative to a 14-electron/Dy pseudogap and large negative pressures on the Dy atoms. Though the $Ga_2$ dumbbell/Ga single atom substitution leading to $Dy_3Ga_{11}$ provides progress in solving both these issues, residual negative pressures on the Dy remain that appear to be severe enough that this otherwise plausible compound does not form. Cu incorporation into the Ga sublattice helps overcome this issue by shrinking the coordination environments of the Dy atoms with the assistance of a block-like incommensurate pattern of dumbbell-single atom substitutions.

A FAST analysis of this situation highlights a competition between the Cu atoms' ability to stabilize the atomic packing around the Dy atoms and its lower valence electron count, which urges a reduction in the dumbbell/single atom substitution. The relatively high Cu/Ga ratio of $Dy(Cu_{0.18}Ga_{0.82})_{3.71(1)}$ indicates that the atomic packing factor plays a larger role in this case, but one could imagine other compromises. In fact, our synthetic exploration of the $Dy(Cu/Ga)_{4-x}$ system has uncovered at least four other modulated compounds where the **q**-vectors change as a function of the nominal Cu:Ga loading ratio, which we are currently pursuing.

These results show how a compound just outside the stability range of a common structure type, $BaAl_4$-type $DyGa_4$, can serve as the source for intriguing structural chemistry when an additional element is added that helps address the issues that destabilize it. It will be interesting to induce structural complexity in other ternary Dy-T-Ga systems, such Dy-Ni-Ga (containing the $Dy_3Ga_{11}$-type phase $DyNi_{2.8}Ga_{8.2}$[67]) or Dy-Zn-Ga, as well as other systems known to undergo CP-drive structural transitions. For instance, replacing Sr in $CaCu_5$-type $SrAg_5$ with Ca leads to the defect structure $Ca_2Ag_7$.[68,69] Going further and adding Mg to the system would be expected to be outside of $CaCu_5$'s stability range and possibly a launching point for intriguing structural chemistry. More broadly, this work points to a general strategy for accessing the farthest reaches of a structure type's stability: FAST analysis of a 'missing' common structure and the addition of an element that solves its issues.

## ASSOCIATED CONTENT

**Supporting Information**. Crystallographic tables for the average and (3+2)D structures of $Dy(Cu_{0.18}Ga_{0.82})_{3.71(1)}$; calculation details for the custom scattering form factors used in the refinement of the Cu/Ga

mixed sites; the MATLAB script used to generate the peak integration list for the (3+2)D model of $Dy(Cu_{0.18}Ga_{0.82})_{3.71(1)}$; powder X-ray diffraction results; energy-dispersive X-ray spectroscopy (EDS) results; additional computational details; comparison of GGA-DFT $DyGa_4$ and $YGa_4$ DOS distributions; comparison of GGA-DFT $Dy_3Ga_{11}$ and $Y_3Ga_{11}$ DOS distributions; CP schemes calculated with free-ion profiles at different percentages of the Bader charge. The Crystallographic Information File (CIF) can be obtained from the Cambridge Crystallographic Data Centre (deposition number: CSD 2000083) and is also provided in the Supporting Information.

## AUTHOR INFORMATION

### Corresponding Author

* email: danny@chem.wisc.edu

### Author Contributions

The manuscript was written through contributions of all authors.

## ACKNOWLEDGMENT

The authors thank Kendall Kamp for discussions about the FAST principle in the Dy-Cu-Ga system and Erdong Lu for his assistance with MATLAB. The authors also acknowledge Bil Schneider for his aid with EDS specimen preparation. We also gratefully acknowledge the financial support of the NSF grant DMR-1809594. H.M.W. thanks the National Science Foundation for a graduate student research fellowship (DGE-1747503). This work includes calculations that used computing resources supported by NSF Grant CHE-0940494.

## REFERENCES

(1) Hertz, M. B.; Baumbach, R. E.; Latturner, S. E. Flux Synthesis of $MgNi_2Bi_4$ and Its Structural Relationship to $NiBi_3$. *Inorg. Chem.* **2020**, *59*, 3452-3458.

(2) Kanatzidis, M. G.; Pöttgen, R.; Jeitschko, W. The Metal Flux: A Preparative Tool for the Exploration of Intermetallic Compounds. *Angew. Chem. Int. Ed.* **2005**, *44*, 6996-7023.

(3) Lupinetti, A. J.; Fife, J. L.; Garcia, E.; Dorhout, P. K.; Abney, K. D. Low-Temperature Synthesis of Uranium Tetraboride by Solid-State Metathesis Reactions. *Inorg. Chem.* **2002**, *41*, 2316-2318.

(4) Rognerud, E. G.; Rom, C. L.; Todd, P. K.; Singstock, N. R.; Bartel, C. J.; Holder, A. M.; Neilson, J. R. Kinetically Controlled Low-Temperature Solid-State Metathesis of Manganese Nitride $Mn_3N_2$. *Chem. Mater.* **2019**, *31*, 7248-7254.

(5) Shemkunas, M. P.; Wolf, G. H.; Leinenweber, K.; Petuskey, W. T. Rapid Synthesis of Crystalline Spinel Tin Nitride by a Solid-State Metathesis Reaction. *J. Am. Ceram. Soc.* **2002**, *85*, 101-104.

(6) Clarke, S. M.; Powderly, K. M.; Walsh, J. P. S.; Yu, T.; Wang, Y.; Meng, Y.; Jacobsen, S. D.; Freedman, D. E. Controlling Dimensionality in the Ni–Bi System with Pressure. *Chem. Mater.* **2019**, *31*, 955-959.

(7) Klein, R. A.; Altman, A. B.; Saballos, R. J.; Walsh, J. P. S.; Tamerius, A. D.; Meng, Y.; Puggioni, D.; Jacobsen, S. D.; Rondinelli, J. M.; Freedman, D. E. High-pressure synthesis of the $BiVO_3$ perovskite. *Phys. Rev. Materials* **2019**, *3*, 064411.

(8) Ulrich, S.; Rodrigo, C.; Julia, M. H.; Aron, W.; Yurii, P.; Matej, B.; Yuri, G. The untypical high-pressure Zintl phase $SrGe_6$. *Z. Naturforsch. B* **2020**, *75*, 209-216.

(9) Samson, S. The crystal structure of the phase β-$Mg_2Al_3$. *Acta Crystallogr.* **1965**, *19*, 401-413.

(10) Andersson, S. An Alternative Description of the Structure of $Cu_4Cd_3$. *Acta Crystallogr. B* **1980**, *36*, 2513-2516.

(11) Samson, S. The Crystal Structure of the Intermetallic Compound $Cu_4Cd_3$. *Acta Crystallogr.* **1967**, *23*, 586-600.

(12) Samson, S. Crystal Structure of $NaCd_2$. *Nature* **1962**, *195*, 259-262.

(13) Yang, Q.-B.; Andersson, S.; Stenberg, L. An Alternative Description of the Structure of $NaCd_2$. *Acta Crystallogr. B* **1987**, *43*, 14-16.

(14) Zhong, Y.; Yang, M.; Liu, Z.-K. Contribution of first-principles energetics to Al–Mg thermodynamic modeling. *Calphad* **2005**, *29*, 303-311.

(15) Pelton, A. D. Cd-Na (Cadmium-Sodium). *Binary Alloy Phase Diagrams, II Ed., Ed. T.B. Massalski* **1990**, *Vol. 2*, 999-1001.

(16) Andress, K. R.; Alberti, E. Roentgenographische Untersuchung der Legierungsreihe Al-Ba. *Z. Metallkd.* **1935**, *27*, 126-128.

(17) Mitchell Warden, H. E.; Fredrickson, D. C. Frustrated and Allowed Structural Transitions: The Theory-Guided Discovery of the Modulated Structure of IrSi. *J. Am. Chem. Soc.* **2019**, *141*, 19424-19435.

(18) Shatruk, M. $ThCr_2Si_2$ structure type: The "perovskite" of intermetallics. *J. Solid State Chem.* **2019**, *272*, 198-209.

(19) Suen, N.-T.; Huang, L.; Meyers, J. J.; Bobev, S. An Unusual Triple-Decker Variant of the Tetragonal $BaAl_4$-Structure Type: Synthesis, Structural Characterization, and Chemical Bonding of $Sr_3Cd_8Ge_4$ and $Eu_3Cd_8Ge_4$. *Inorg. Chem.* **2018**, *57*, 833-842.

(20) Gout, D.; Barker, T. J.; Gourdon, O.; Miller, G. J. A New Superstructure for the $BaAl_4$-Structure Type: An Experimental and Theoretical Study of $La_2NiAl_7$. *Chem. Mater.* **2005**, *17*, 3661-3667.

(21) Grin, Y.; Ellner, M.; Predel, B.; Baumgartner, B. Crystal Structure of $CaCu_{0.15}Ga_{3.85}$—A New Variant of the $BaAl_4$ Structure Type: Structure Analysis from X-Ray Powder Diffraction Data. *J. Solid State Chem.* **1995**, *114*, 342-345.

(22) Markiv V.Y., S. I. P., Belyavina N.N., and Kuz'menko P.P. Phase equilibria (500 °C) in the Dy-Cu-Ga system and new compounds with the BaAl4-type structrue and its derivatives in the RE-Cu-Ga systems. *Dopov. Akad. Nauk Ukr. RSR, Ser. A* **1985**, *7*, 76-81.

(23) Amerioun, S.; Häussermann, U. Structure and Bonding of $Sr_3In_{11}$: How Size and Electronic Effects Determine Structural Stability of Polar Intermetallic Compounds. *Inorg. Chem.* **2003**, *42*, 7782-7788.

(24) Zheng, C.; Hoffmann, R. An Unusual Electron Count and Electron-Deficient Multi-Center Bonding in One Class of Intermetallics: The $BaAl_4$, $CaAl_2Zn_2$, $CeMg_2Si_2$ and FCC Al Structures. *Z. Naturforsch. B* **1986**, *41*, 292-320.

(25) Lin, Q.; Miller, G. J.; Corbett, J. D. Ordered $BaAl_4$-Type Variants in the $BaAu_xSn_{4-x}$ System: A Unified View on Their Phase Stabilities versus Valence Electron Counts. *Inorg. Chem.* **2014**, *53*, 5875-5877.

(26) Häussermann, U.; Amerioun, S.; Eriksson, L.; Lee, C.-S.; Miller, G. J. The s–p Bonded Representatives of the Prominent $BaAl_4$ Structure Type: A Case Study on Structural Stability of Polar Intermetallic Network Structures. *J. Am. Chem. Soc.* **2002**, *124*, 4371-4383.

(27) Perdew, J. P.; Chevary, J. A.; Vosko, S. H.; Jackson, K. A.; Pederson, M. R.; Singh, D. J.; Fiolhais, C. Atoms, molecules, solids, and surfaces: Applications of the generalized gradient approximation for exchange and correlation. *Phys. Rev. B* **1992**, *46*, 6671-6687.

(28) Perdew, J. P.; Chevary, J. A.; Vosko, S. H.; Jackson, K. A.; Pederson, M. R.; Singh, D. J.; Fiolhais, C. Erratum: Atoms, molecules, solids, and surfaces: Applications of the generalized gradient approximation for exchange and correlation. *Phys. Rev. B* **1993**, *48*, 4978-4978.

(29) Kresse, G.; Furthmüller, J. Efficient iterative schemes for ab initio total-energy calculations using a plane-wave basis set. *Phys. Rev. B* **1996**, *54*, 11169-11186.

(30) Kresse, G.; Furthmüller, J. Efficiency of ab-initio total energy calculations for metals and semiconductors using a plane-wave basis set. *Comput. Mater. Sci* **1996**, *6*, 15-50.

(31) Kresse, G.; Hafner, J. Ab initio molecular dynamics for liquid metals. *Phys. Rev. B* **1993**, *47*, 558-561.
(32) Kresse, G.; Hafner, J. Ab initio molecular-dynamics simulation of the liquid-metal—amorphous-semiconductor transition in germanium. *Phys. Rev. B* **1994**, *49*, 14251-14269.
(33) Blöchl, P. E. Projector augmented-wave method. *Phys. Rev. B* **1994**, *50*, 17953.
(34) Kresse, G.; Joubert, D. From ultrasoft pseudopotentials to the projector augmented-wave method. *Phys. Rev. B* **1999**, *59*, 1758-1775.
(35) Landrum, G. A.; Glassey, W. V. YAeHMOP: Yet Another Extended Hückel Molecular Orbital Package, YAeHMOP is freely available via the Internet at URL: https://sourceforge.net/projects/yaehmop/.
(36) Gonze, X. A brief introduction to the ABINIT software package. *Z. Kristallog. – Cryst. Mater.* **2005**, *220*, 558-562.
(37) Gonze, X.; Amadon, B.; Anglade, P. M.; Beuken, J. M.; Bottin, F.; Boulanger, P.; Bruneval, F.; Caliste, D.; Caracas, R.; Côté, M.; Deutsch, T.; Genovese, L.; Ghosez, P.; Giantomassi, M.; Goedecker, S.; Hamann, D. R.; Hermet, P.; Jollet, F.; Jomard, G.; Leroux, S.; Mancini, M.; Mazevet, S.; Oliveira, M. J. T.; Onida, G.; Pouillon, Y.; Rangel, T.; Rignanese, G. M.; Sangalli, D.; Shaltaf, R.; Torrent, M.; Verstraete, M. J.; Zerah, G.; Zwanziger, J. W. ABINIT: First-principles approach to material and nanosystem properties. *Comput. Phys. Commun.* **2009**, *180*, 2582-2615.
(38) Gonze, X.; Beuken, J. M.; Caracas, R.; Detraux, F.; Fuchs, M.; Rignanese, G. M.; Sindic, L.; Verstraete, M.; Zerah, G.; Jollet, F.; Torrent, M.; Roy, A.; Mikami, M.; Ghosez, P.; Raty, J. Y.; Allan, D. C. First-principles computation of material properties: the ABINIT software project. *Comput. Mater. Sci* **2002**, *25*, 478-492.
(39) Hartwigsen, C.; Goedecker, S.; Hutter, J. Relativistic separable dual-space Gaussian pseudopotentials from H to Rn. *Phys. Rev. B* **1998**, *58*, 3641-3662.
(40) Hilleke, K. P.; Fredrickson, D. C. Discerning Chemical Pressure amidst Weak Potentials: Vibrational Modes and Dumbbell/Atom Substitution in Intermetallic Aluminides. *J. Phys. Chem. A* **2018**, *122*, 8412-8426.
(41) Berns, V. M.; Engelkemier, J.; Guo, Y.; Kilduff, B. J.; Fredrickson, D. C. Progress in Visualizing Atomic Size Effects with DFT-Chemical Pressure Analysis: From Isolated Atoms to Trends in $AB_5$ Intermetallics. *J. Chem. Theory Comput.* **2014**, *10*, 3380-3392.
(42) Bader, R. F. W. *Atoms in Molecules: A Quantum Theory*; Oxford; New York: Clarendon Press, 1990.
(43) Henkelman, G.; Arnaldsson, A.; Jónsson, H. A fast and robust algorithm for Bader decomposition of charge density. *Comput. Mater. Sci* **2006**, *36*, 354-360.
(44) Sanville, E.; Kenny, S. D.; Smith, R.; Henkelman, G. Improved grid-based algorithm for Bader charge allocation. *J. Comput. Chem.* **2007**, *28*, 899-908.
(45) Tang, W.; Sanville, E.; Henkelman, G. A grid-based Bader analysis algorithm without lattice bias. *J. Phys.: Condens. Matter* **2009**, *21*, 084204.
(46) Oliveira, M. J. T.; Nogueira, F. Generating relativistic pseudo-potentials with explicit incorporation of semi-core states using APE, the Atomic Pseudo-potentials Engine. *Comput. Phys. Commun.* **2008**, *178*, 524-534.
(47) Drake, B. L.; Capan, C.; Cho, J. Y.; Nambu, Y.; Kuga, K.; Xiong, Y. M.; Karki, A. B.; Nakatsuji, S.; Adams, P. W.; Young, D. P.; Chan, J. Y. Crystal growth, structure, and physical properties of $Ln(Cu,Al)_{12}$ (Ln = Y, Ce, Pr, Sm, and Yb) and $Ln(Cu,Ga)_{12}$ (Ln = Y, Gd–Er, and Yb). *J. Phys.: Condens. Matter* **2010**, *22*, 066001.
(48) Agilent. *CrysAlis PRO*. Agilent Technologies Ltd, Yarnton, Oxfordshire, England. **2014**.
(49) Oszlányi, G.; Sütő, A. Ab initio structure solution by charge flipping. *Acta Crystallogr. A* **2004**, *60*, 134-141.
(50) Oszlányi, G.; Sütő, A. Ab initio structure solution by charge flipping. II. Use of weak reflections. *Acta Crystallogr. A* **2005**, *61*, 147-152.
(51) Palatinus, L.; Chapuis, G. SUPERFLIP - a computer program for the solution of crystal structures by charge flipping in arbitrary dimensions. *J. Appl. Crystallogr.* **2007**, *40*, 786-790.
(52) Petříček, V.; Dušek, M.; Palatinus, L. Crystallographic Computing System JANA2006: General features. *Z. Kristallog. – Cryst. Mater.* **2014**, *229*, 345-352.
(53) *International Tables for Crystallography Volume C: Mathematical, physical and chemical tables*; Prince, E., Ed.; Chester, England : International Union of Crystallography, 2006.
(54) Kripyakevich, P. I.; Gladyshevskii, E. I.; Dzyana, D. I. Binary intermetallic compounds of the $BaAl_4$ type containing gallium. *Kristallografiya* **1965**, *10*, 471-473.
(55) Bruzzone, G. $MX_4$ compounds of alkaline earth metals with IIIB group elements. *Acta Crystallogr.* **1965**, *18*, 1081-1082.
(56) Buschow, K. H. J.; van Vucht, J. H. N. Systematic arrangement of the binary rare-earth-aluminium systems. *Philips Res. Rep.* **1967**, *22*, 233-245.
(57) Buschow, K. H. J. The lanthanum - aluminum system. *Philips Res. Rep.* **1965**, *20*, 337-348.
(58) Ao, W. Q.; Li, J. Q.; Jian, Y. X.; Liu, F. S.; Zhuang, Y. H. Reinvestigation of the phase diagram of the Dy–Ga binary system. *Calphad* **2007**, *31*, 233-236.
(59) Peterson, G. G. C.; Geisler, E. E.; Fredrickson, D. C. Intermetallic Reactivity: $Ca_3Cu_{7.8}Al_{26.2}$ and the Role of Electronegativity in the Stabilization of Modular Structures. *Inorg. Chem.* **2020**, *59*, 5018-5029.
(60) de Wolff, P. M. The Pseudo-Symmetry of Modulated Crystal Structures. *Acta Crystallogr. A* **1974**, *30*, 777-785.
(61) Van Smaalen, S. Incommensurate crystal structures. *Crystallogr. Rev.* **1995**, *4*, 79-202.
(62) van Smaalen, S.; Campbell, B. J.; Stokes, H. T. Equivalence of superspace groups. *Acta Crystallogr. A* **2013**, *69*, 75-90.
(63) Stokes, H. T.; Campbell, B. J.; van Smaalen, S. Generation of (3 + d)-dimensional superspace groups for describing the symmetry of modulated crystalline structures. *Acta Crystallogr. A* **2011**, *67*, 45-55.
(64) Stokes, H. T.; Hatch, D. M.; Campbell, B. J. ISO(3+d)D, ISOTROPY Software SUITE, iso.byu.edu.
(65) Lidin, S.; Piao, S. $Cu_5In_3$-$Cu_3In_2$ Revisited. *Eur. J. Inorg. Chem.* **2018**, *2018*, 3548-3553.
(66) Harmonic modeling of the occupations leads to small regions where the sum occupancy for a dumbbell/single atom site pair is < 0 or > 1. In these cases, the occupation was set to 0 or 1, respectively, for the weighting scheme.
(67) Vasilechoko, L. O.; Grin, Y. Phase equilibria in the Dy-Ni-Ga system at 600 °C. *Inorg. Mater.* **1996**, *32*, 512-515.
(68) Snyder, G. J.; Simon, A. Crystal structure of $Ag_7Ca_2$ — a new intermetallic structure type. *J. Alloys Compd.* **1995**, *223*, 65-69.
(69) Berns, V. M.; Fredrickson, D. C. Structural Plasticity: How Intermetallics Deform Themselves in Response to Chemical Pressure, and the Complex Structures That Result. *Inorg. Chem.* **2014**, *53*, 10762-10771.

For Table of Contents Use Only

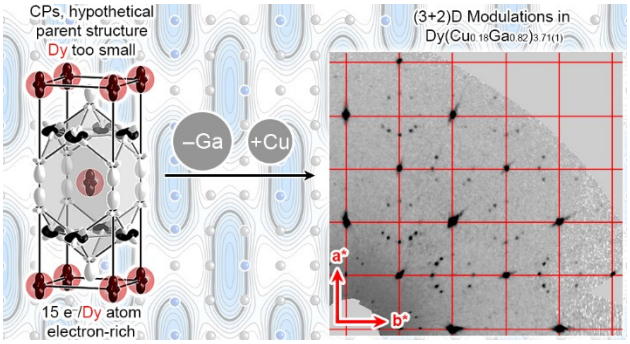


**Synopsis:** We apply the FAST principle to investigating the complexity that emerges at the compositional limits of the $BaAl_4$ type. Theoretical analysis of the unobserved but plausible $BaAl_4$-type $DyGa_4$ trace its instability of $DyGa_4$ to an excess of electrons and overly large Dy coordination environments. Cu incorporation and dumbbell/single atom substitution represent overlapping routes to addressing these issues. In the 2D incommensurately modulated structure of $Dy(Cu_{0.18}Ga_{0.82})_{3.71(1)}$, these factors are realized in a checkerboard-pattern of $La_3Al_{11}$-type domains.